CrossMark

Representation of monsoon intraseasonal oscillations in regional climate model: sensitivity to convective physics

U. Umakanth[1] · Amit P. Kesarkar[1] · Attada Raju[2,3] · S. Vijaya Bhaskar Rao[4]

Abstract The aim of the study is to evaluate the performance of regional climate model (RegCM) version 4.4 over south Asian CORDEX domain to simulate seasonal mean and monsoon intraseasonal oscillations (MISOs) during Indian summer monsoon. Three combinations of Grell (G) and Emanuel (E) cumulus schemes namely, RegCM-EG, RegCM-EE and RegCM-GE have been used. The model is initialized at 1st January, 2000 for a 13-year continuous simulation at a spatial resolution of 50 km. The models reasonably simulate the seasonal mean low level wind pattern though they differ in simulating mean precipitation pattern. All models produce dry bias in precipitation over Indian land region except in RegCM-EG where relatively low value of dry bias is observed. On seasonal scale, the performance of RegCM-EG is more close to observation though it fails at intraseasonal time scales. In wave number-frequency spectrum, the observed peak in zonal wind (850 hPa) at 40–50 day scale is captured by all models with a slight change in amplitude, however, the 40–50 day peak in precipitation is completely absent in RegCM-EG. The space–time characteristics of MISOs are well captured by RegCM-EE over RegCM-GE, however it fails to show the eastward propagation of the convection across the Maritime Continent. Except RegCM-EE all other models completely underestimates the moisture advection from Equatorial Indian Ocean onto Indian land region during life-cycle of MISOs. The characteristics of MISOs are studied for strong (SM) and weak (WM) monsoon years and the differences in model performances are analyzed. The wavelet spectrum of rainfall over central India denotes that, the SM years are dominated by high frequency oscillations (period <20 days) whereas little higher periods (>30 days) along with dominated low periods (<20 days) observed during WM years. During SM, RegCM-EE is dominated with high frequency oscillations (period <20 days) whereas in WM, RegCM-EE is dominated with periods >20 days. Except RegCM-EE, all other models fail to capture the observed spectral features for SM and WM years.

Keywords Regional climate model · Seasonal mean monsoon · Intraseasonal variability of the monsoon · Active and break spells · Horizontal moisture advection

1 Introduction

Indian Summer Monsoon (ISM) is one of the spectacular features of the global atmospheric general circulation, and is important due to its impact on agrarian economies of countries like India. The country receives more than 80 % of its annual precipitation during June to September (JJAS) of ISM (Rajeevan et al. 2013). The ISM exhibits large amplitude sub-seasonal variability dominated by quasi-periodic oscillations known as the monsoon intraseasonal oscillations (MISOs). The MISOs are characterized by fluctuations of the Tropical Convergence Zone (TCZ) between central equatorial Indian Ocean and the monsoon trough over Indian land within season. The slowly evolving northward propagating MISOs are associated with episodes

✉ U. Umakanth
  umakanth@narl.gov.in

[1] National Atmospheric Research Laboratory, Gadanki, Andhra Pradesh 517112, India

[2] Indian Institute of Tropical Meteorology, Pune, India

[3] King Abdullah University of Science and Technology, Thuwal, Saudi Arabia

[4] Department of Physics, Sri Venkateswara University, Tirupati 517502, India

of quasi-periodic active spells (prolonged abundant precipitation), punctuated by break spells (prolonged reduced precipitation) (Rajeevan et al. 2010; Umakanth et al. 2014). These are dominant at 30–50 day period in ISM region and they determine the strength of the seasonal mean monsoon (e.g. Yasunari 1979, 1980; Sikka and Gadgil 1980; Goswami and Ajaya Mohan 2001; Goswami et al. 2006). Therefore, the proper simulation of MISOs in the state-of-the-art climate models is very important for short and long-term prediction of the ISM.

In the last four decades a significant advancement has been achieved in understanding the structure and underlying mechanisms for the northward propagating 30–50 day monsoon intraseasonal mode using both observation and numerical models (e.g. Krishnamurti and Subrahmanyam 1982; Goswami and Shukla 1984; Lawrence and Webster 2002; Jiang et al. 2004; Wang et al. 2006; references therein). The current generation General Circulation Models (GCMs) have poor skill in simulating seasonal mean precipitation distribution mostly over precipitation prone regions such as west coast of India, the head Bay of Bengal and northeast India (e.g. Kripalani et al. 2007). This is likely caused by improper representation of regional forcing such as Himalayan highlands and the Western Ghats due to their coarser grid resolution (e.g. Krishna Kumar et al. 2005; Rupa Kumar et al. 2006; Raju et al. 2015a, b). In addition to that, the current status of MISOs representation in global models is still limited due to model deficiencies (e.g. Fu et al. 2003; Waliser et al. 2003; Fu and Wang 2004; Rajendran et al. 2004; Wang et al. 2006). Therefore, in order to study the seasonal mean and intraseasonal variability associated with ISM at high spatial and temporal resolutions, a novel approach is to use a regional climate model (RCM) (e.g. Giorgi 2006). The idea behind using RCMs is to improve the regional features by allowing resolved convective processes of ISM simulated by global models (e.g. AGCM/CGCM). A number of studies have been carried out to test the ability of RCMs to simulate annual and seasonal mean ISM features using GCMs/reanalysis data as lateral boundary conditions (e.g. Bhaskaran et al. 1996; Vernekar and Ji 1999; Ratnam and Krishna Kumar 2005; Dash et al. 2006; Philippe et al. 2011; Raju et al. 2015a, b; references therein). The above studies indicated that the improvement in the simulation of spatial and temporal distribution of mean monsoon precipitation characteristics is due to the better representation of orography, land cover and land-sea contrasts in regional models.

The RegCM developed at International Center for Theoretical Physics (ICTP), is one of the widely used regional climate models and it has been employed for various studies (e.g. Dash et al. 2006; Giorgi et al. 2012; Maharana

and Dimri 2015; Raju et al. 2015a, b). It is noteworthy to mention that this model is one of the state-of-the-art RCM members in COordinated Regional climate Downscaling Experiment (CORDEX). Therefore, evaluating the ISM elements at seasonal and intraseasonal scales will provide useful information for further improvement in convective parameterization schemes. It is important to emphasize that the cumulus convection scheme is known to have an important role in MISO simulation because the coupling between convection and circulation is a key process in MISO (e.g. Zhang and Mu 2005) and seasonal mean climate (e.g. Byun and Hong 2004). Dash et al. (2006) has found that Grell cumulus scheme over land and Emanuel cumulus scheme over Ocean is best in simulating the seasonal mean and variability in precipitation distribution during ISM. On the other hand, recent study indicating that a mixed scheme (Emanuel over land and Grell over ocean) is better in simulating precipitation realistically over ISM (Raju et al. 2015a, b). The RCM studies concludes that the performance of some cumulus parameterization schemes do not seem to work well always over Asian monsoon region (e.g. Leung et al. 1999). This different model behavior might be true because the performance of model always changes accordingly with improved physics in the model. Moreover, simulation of monsoon with RCMs was found to be very sensitive to different cumulus parameterization schemes, particularly over the monsoon region where convection plays a major role in monsoon dynamics (e.g. Dash et al. 2006). Hence, thorough evaluation of model convective physics is essential. Maharana and Dimri (2015) evaluated RegCM with Grell cumulus scheme for the simulation of monsoon intraseasonal variability associated with active and break spells of ISM. Their analysis is mainly focused on active and break spells over Indian land region based on single convective scheme.

Keeping these aspects in background, in this paper, we utilize RegCM4.4 which is comprised with a number of new features including improvements to the physics packages that enhance model performance. Instead of having a fixed combination of cumulus schemes, we have examined model sensitivity to different combinations of cumulus schemes. The primary objective of this paper is to assess suitable combination of convection schemes in RegCM4.4 for the simulation of seasonal mean and MISOs during ISM over South Asian CORDEX domain. The paper is organized is as follows. Brief description of model used is given in Sect. 2.1, followed by Sect. 2.2 providing the details of model experiments and data and methodology. Section 3 demonstrates the seasonal mean ISM features and intra-seasonal oscillations are examined in Sect. 4. The summary and conclusions are presented in Sect. 5.

2 Model description, experiment design, data and methodology

2.1 Model description

The model used in this study is RegCM4.4 which is available at ICTP for various studies, from seasonal to climate change simulation. It has the capability of running different combinations of convection schemes over land as well as ocean, referred as mixed convection schemes. Giorgi et al. (2012) suggests that the mixed convection approach might be better in climate scale simulation over CORDEX domain. RegCM4.4 includes a number of new features including improvements in the model physics that enhance model performance in tropical and subtropical regions as compared to the previous versions (Giorgi et al. 2012). Therefore, RegCM4.4 is used worldwide to simulate the regional-scale climatology for all possible scales which provide insights into the regional climate processes.

The model is a hydrostatic, compressible, terrain following sigma-p vertical coordinate model running on an Arakawa B-grid in which wind and thermodynamical variables are horizontally staggered (Giorgi et al. 1993a, b; Pal et al. 2007). In the present study, we have chosen mixed combination of Grell (1993) and Emanuel (1991) cumulus schemes. Fundamentally, Grell scheme includes two closure assumptions: an Arakawa-Schubert in which buoyant energy is immediately released at each time step and Fritsch-Chappell type in which all available buoyant energy (CAPE) dissipates at a specified time step of 30 min (Giorgi et al. 2012). The Emanuel scheme assumes that mixing in clouds is highly inhomogeneous and episodic. Modeling of convective fluxes is based on an idealized condition of sub-cloud-scale down drafts and updrafts. The process of convection is initiated if the level of neutral buoyancy is greater than the cloud base level. For land surface process representation, we have used Community Land Model version CLM4.5 which is the major addition in RegCM4.4 (Oleson et al. 2008). NCAR's global community climate model version CCM3 (Kiehl et al. 1996) has been chosen for radiative transfer calculation. Resolved scale precipitation scheme which includes prognostic equation for cloud water is based on sub grid explicit moisture (SUBEX) parameterization of Pal et al. (2000). A new PBL scheme which is UW-PBL (University of Washington) from University of Washington was implemented in RegCM4.4 and is currently used in the study (Grenier and Bretherton 2001).

2.2 Experimental design

In this study we have considered South Asian CORDEX domain which covers a region of 19°S–43°N and 6°°E–130°E. The experiments have been conducted with a horizontal resolution of 50 km i.e. 151 × 273 points along east–west and north–south direction and 23 sigma levels in vertical under Mercator projection. We have chosen Grell and Emanuel cumulus schemes and the model is run with two mixed convective schemes i.e. Grell over land and Emanuel over Ocean (RegCM-GE), Emanuel over land and Grell over ocean (RegCM-EG) and one with Emanuel for both land and ocean (RegCM-EE). The initial and lateral boundary conditions are obtained from European Center for Medium Range Weather Forecast (ECMWF) reanalysis (ERA15) data with a grid spacing of 1.5° × 1.5° at every 6 h and the surface boundary conditions are obtained from National Oceanic and Atmospheric Administration (NOAA) Optimum Interpolation Sea Surface Temperature (OISST) at 1° × 1° resolution. Geophysical parameters are obtained from United States Geological Survey (USGS). The model is initialized from 1st January 2000 and is allowed to run continuously for a period of 13-years. The initial year (i.e. 2000) is used as model spin-up, which is sufficient for the dynamical equilibrium between the lateral forcing and the internal physics and dynamics of the model (Anthes et al. 1989). In this study, analysis is considered from 2001 to 2012 (12 years).

2.3 Data and methodology

Global Precipitation Climatology Project (GPCP) precipitation data (Huffman et al. 2001) available at 1° × 1° grid resolution at daily scale has been used for the period 2001–2012 to validate the model precipitation. The data has been developed by optimally merging estimates computed from microwave, infrared, and sounder data observed by the international constellation of precipitation related satellites, and rain gauge data from more than 6000 stations. In order to assess the large scale features simulated by the model, we have used high resolution ERA-interim 0.5° × 0.5° gridded reanalysis data for the period of study. The ERA-interim reanalysis is the third generation ECMWF reanalysis product with 4-D variational analysis, a better formulation of background error constraint than ERA-40 reanalysis product (e.g. Dee et al. 2011). It has good coverage of upper-air measurements over the whole globe and is regarded as relatively more reliable reanalysis datasets (Lin et al. 2014), especially over the Northern Hemisphere. In this study, we have used winds (zonal and meridional), vertical pressure velocity (ω), and specific humidity (q) from ERA-interim reanalysis to compare the circulation and moisture distribution simulated by the model.

The daily anomalies of each meteorological field are computed by subtracting the climatologically mean annual cycle with three harmonics from both observed dataset and

the model output. For extracting monsoon intraseasonal oscillation, 25–90 day band-pass filter (Duchon 1979) is applied on the daily anomalies in order to isolate it from 10–20 day oscillation and is applied for both observation and model. A reference time series is obtained by averaging the filtered precipitation anomalies over central Indian (CI) region (70°E–90°E and 18°N–28°N) and it is standardized by its own standard deviation. The break spells are identified as the period during which the standardized rainfall anomaly is less than −1.0 consecutively for 3 days or more. Similarly the active spells are identified as the periods during which the standardized rainfall anomaly is more than +1.0 consecutively for 3 days or more. This is known as intraseasonal oscillation (ISO) index (e.g. Goswami and Xavier 2003) which is used for identification of active/break spells during peak monsoon months (July and August) in order to avoid late onset and early withdrawal effects. Lag composite and lag regression analysis have been carried out to observe the space–time characteristics of MISOs simulated by the model experiments. The lag composites of 25–90 day filtered precipitation anomalies are obtained based on ISO index. The identified MISO events are composited at different lags for temporal evolution of MISOs. Lag regression analysis is performed by least square fitting the precipitation anomalies with respect to standardized ISO index at different lags and these anomalies are averaged over Indian longitudes (70°E–90°E) in order to observe the origin and the phase propagation of MISOs in northward direction.

3 Simulation of ISM mean state

We first examine how well the seasonal mean ISM features are simulated by the model during the boreal summer with different cumulus schemes. Figure 1 depicts the observed and model simulated mean lower tropospheric monsoon circulation (850 hPa) and precipitation along with model bias estimated against observed seasonal mean precipitation and wind over ISM. Figure 1a, depicts several major circulation features of monsoon including the lower level monsoonal flow, the cross-equatorial Somali jet and the northeast trade winds. These large scale circulation features are captured reasonably well by all three of the cumulus schemes (Fig. 1b–d), though the magnitude of the simulated low-level winds varies differently over land and the ocean (Fig. 1e, f). It is important to mention that well organized cyclonic circulation over CI region (known as monsoon trough region) along the Indo-Gangetic plains is produced in RegCM-EG (Fig. 1b) similar to observations (Fig. 1a) and this feature is weaker in other convective schemes RegCM-GE (Fig. 1c) and RegCM-EE (Fig. 1d). Among the models, RegCM-EG shows unrealistic

movement of monsoon flow at the equator compared to that of observations. Further, the wind biases (Fig. 1e–g) showed that the core of Somali jet and south westerlies over Arabian Sea (AS) is weaker in RegCM-EE (Fig. 1f) and RegCM-GE (Fig. 1g) than RegCM-EG (Fig. 1e). These wind biases in all the models are consistent with sea level pressure biases (Figure not shown) in the model experiments. It is known that the tropospheric temperature (TT) gradient (averaged between 700–400 hPa) is primarily responsible for deep ISM circulation during ISM (Webster et al. 1998). The strength of the ISM is closely related to the sign of the meridional gradient of TT (the difference of TT values between the northern box 40°–100°E; 5°–35°N and the southern box 40°–100°E; 15°S–5°N). All models simulated the seasonal evolution of TT gradient reasonably well compared to observation; however, RegCM-EG produced the TT gradient relatively close to the observed TT gradient with correlation coefficient (CC) of 0.95 (Figure not shown). Therefore, on the whole, the RegCM-EG has shown relatively good performance to simulate TT gradient which reflects in the better simulation of monsoon circulation. Overall, the predominant southwesterly flow across the AS and a large-scale cyclonic flow extending from the Bay of Bengal (BoB) to the northwest India can influence the precipitation distribution.

Observations (Fig. 1a) show the presence of regional convective centers such as Western Ghats, CI, the head Bay of Bengal (BoB), Equatorial Indian Ocean (EIO) belt (Equator to 10°S) over ISM region. Previous studies have shown that the interannual variability of ISM precipitation depends on the relative time in which one of these zones is more active, and is primarily governed by the intraseasonal oscillation of ISM (e.g. Goswami and Ajaya Mohan 2001). All models produce the main features of precipitation distribution, such as the two maxima on either side of the Indian peninsula. In particular, RegCM-EG (Fig. 1b) shows CI region precipitation, rain shadow region over the southeastern India apart from precipitation maxima. In contrast, RegCM-EE (Fig. 1c) and RegCM-GE (Fig. 1d) have few deficiencies in producing precipitation over these regions. All models failed to simulate location of maximum rainfall band over the head BoB region. It seems that the model simulated rainfall is restricted to central/southern BoB which causes the dry bias over Myanmar coast. However, the wet bias over the southern BoB may possibly be a consequence of the restricted maximum rainfall zone (ITCZ). Unrealistic Inter Tropical Convergence Zone (ITCZ) pattern is evident in the region south of equator in RegCM-EE (Fig. 1c) and RegCM-GE (Fig. 1d) during monsoon. This feature is most common in all types of climate models and surprisingly this unrealistic ITCZ type precipitation is not seen in RegCM-EG (Fig. 1b) which is in accordance with observations. This model behavior may

JJAS Mean rainfall & wind
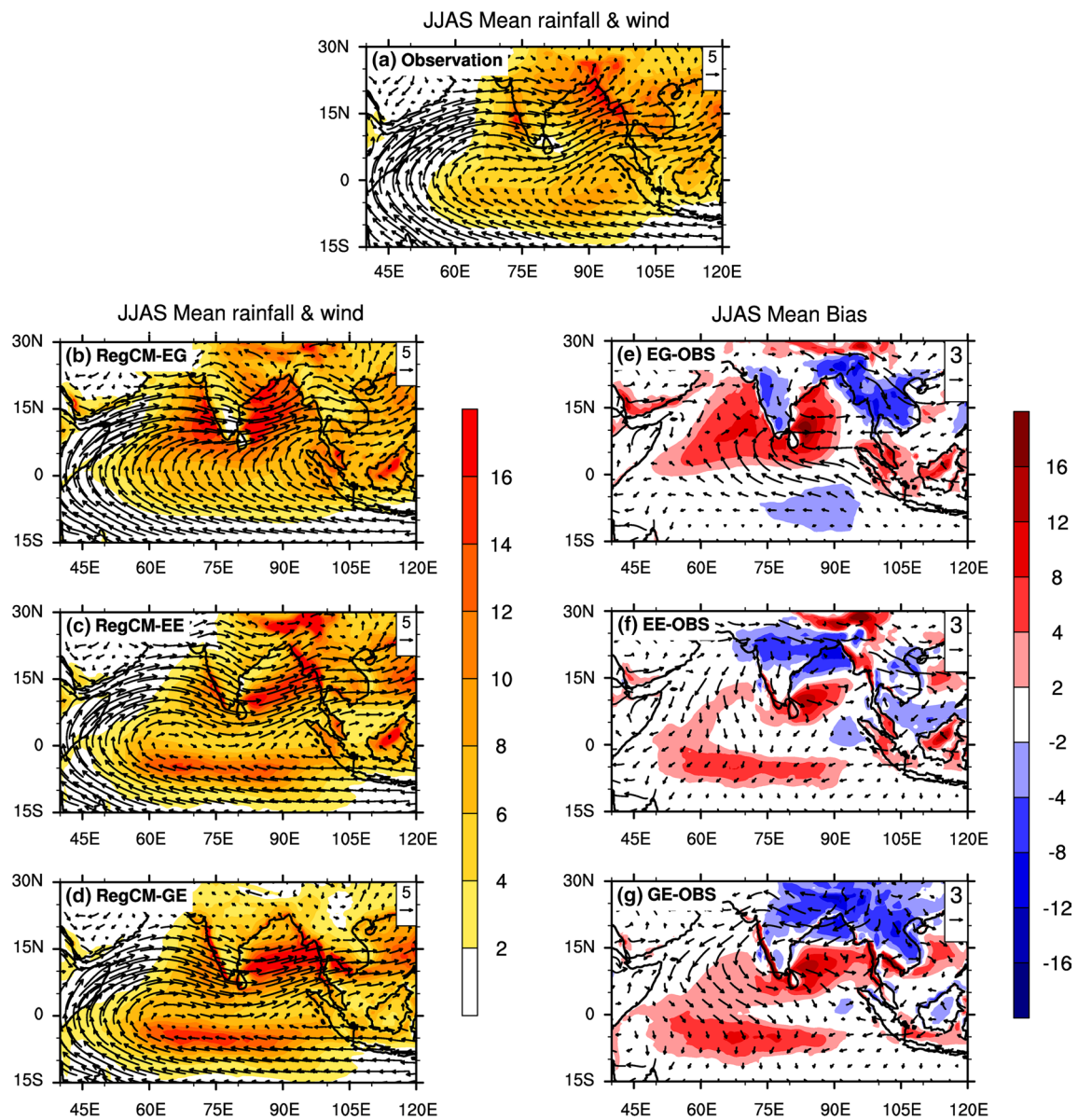
Fig. 1 Seasonal (JJAS) mean precipitation (*shaded*, mm day^{-1}) and low level circulation (*vectors*, m s^{-1}) at 850 hPa for **a** Observation, **b** RegCM-EG, **c** RegCM-EE, **d** RegCM-GE. Similarly mean model bias (**e**, **f**, **g**) against observed precipitation (*Shaded*: *blue* → *red*, mm day^{-1}) and low level circulation (*vectors*, m s^{-1})

be due to the convective schemes and the associated parameters in the model which determine the response of the convection to large-scale atmospheric forcing (Wu et al. 2003). Therefore, this particular aspect demands more sensitivity experiments with cumulus parameters with a focus to reduce the bias simulated by the models. It is important to note that the models (RegCM-EE and RegCM-EG) capture the finer details of orography precipitation along the Himalayan foothills, which are not seen in RegCM-GE (Fig. 1d). Overall, the simulated precipitation exhibits large difference in their spatial distribution i.e. the precipitation is overestimated over EIO and is underestimated over Indian

subcontinent where as in RegCM-EG (Fig. 1e) the overestimation is mostly observed over southern BoB and AS regions. On the whole, RegCM-EE (Fig. 1f) and RegCM-GE (Fig. 1g) produces less precipitation over CI region and more precipitation over EIO while RegCM-EG has underestimation in precipitation over EIO (Fig. 1e).

The precipitation distribution in Fig. 1 gives the average picture of precipitation accumulation during the ISM season. However, its morphology in terms of the onset, sustenance, and withdrawal phases of ISM may be assessed through the space–time evolution of precipitation. In order to examine the model fidelity in simulating the time

evolution of precipitation over CI, the daily precipitation climatology is computed for the period of 2001–2012 (Fig. 2a). The RegCM-EG simulated seasonal cycle is compared with GPCP observed precipitation with CC of 0.81. It is clearly observed in Fig. 2b that the monsoon is fully established in June over Indian continent, continues to shift northward (gradually) thereafter, and withdraws quickly in September in RegCM-EG as in GPCP. On the other hand, RegCM-EE and RegCM-GE underestimated the seasonal cycle which clearly indicates that both convective schemes produced strong dry bias over land region (Fig. 1f, g). The CC of precipitation in RegCM-EE is 0.49 and RegCM-GE is 0.68 against observations. The time-latitude section of daily precipitation over CI in observations shows maximum rain band migrates up to 27°N (Fig. 2b) during the peak monsoon months of July and August (Fig. 2b). The seasonal evolution of northward propagation of maximum rain band is found to be reasonably good in RegCM-EG (Fig. 2c) than RegCM-EE (Fig. 2d) and RegCM-GE (Fig. 2e) simulations compared to that of observations. The northward migration of ITCZ in both RegCM-EE and RegCM-GE is confined to near equatorial latitudes, and it could be a possible reason for dry bias observed over CI region. According to Jiang et al. (2004), the mean easterly shear is one of the key parameter for the northward migration of the convection band at seasonal scale. Our analysis indicates that RegCM-EE and RegCM-GE (RegCM-EG) overestimated (underestimated) the strength of the easterly shear over the ISM region (Figure not shown). These model deficiencies may be responsible for the limitation of northward migration of ITCZ in model which produced maximum rainfall over Southern BoB, subsequently misses the maximum rainfall band along the Myanmar coast. From the above analyses, it appears that RegCM-EG (Fig. 2b) is able to reproduce spatial and temporal precipitation features that are closer to the observations as compared to other schemes at seasonal scale.

In order to identify the model deficiencies for realistic simulation of precipitation, we have examined the mean ISM Hadley circulation for observations and model simulations. Since, the ISM circulation is basically a convectively coupled phenomenon and therefore the large-scale circulation biases would imply on monsoon convection and its associated precipitation. For instance, the dry bias observed in model simulations over CI region may likely be related with local Hadley circulation (monsoon dynamics) at seasonal time scales (e.g. Slingo and Annamalai 2000). The analysis of the meridional and vertical wind associated with the monsoon averaged over Indian longitudes (70°E–90°E) is shown in Fig. 3. It is observed that strong ascending motion around 15°N which is associated with the ISM convective activity, along with a secondary branch of upward motion over the near-equatorial region associated with the
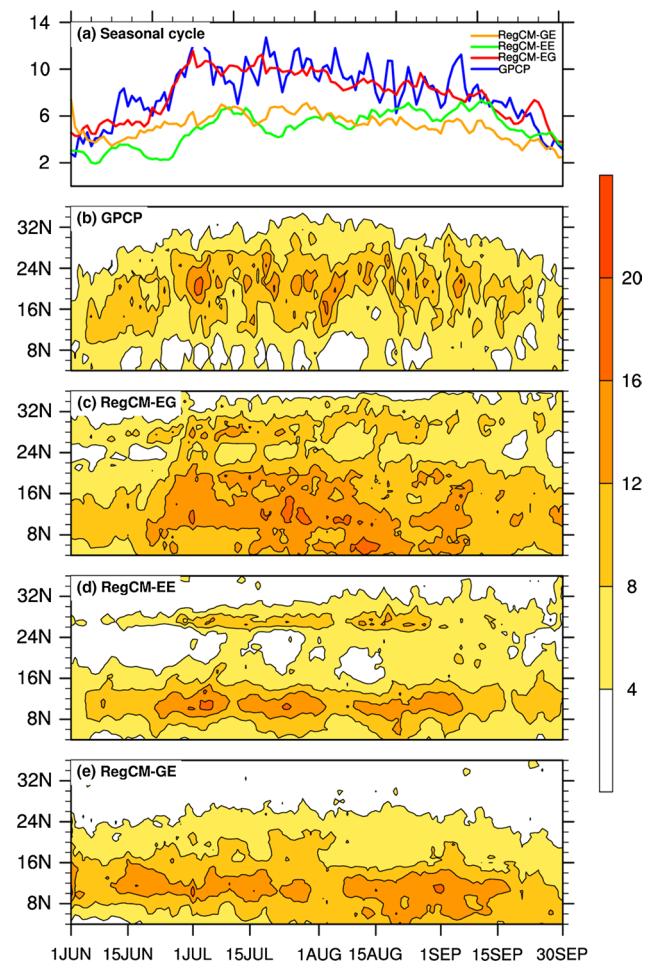
Fig. 2 **a** Seasonal evolution of area averaged precipitation (mm day^{-1}) over CI (70°E–90°E and 18°N–28°N) region and the time-latitude section of precipitation (mm day^{-1}; *shaded*) averaged over Indian longitudes (70–90°E) for **b** GPCP, **c** RegCM-EG, **d** RegCM-EE, **e** RegCM-GE

oceanic TCZ (Fig. 3a). The descending branch of the monsoon Hadley circulation is seen over the southern Indian Ocean and is characterized by strong subsidence around 10°S–20°S latitude belt. The model simulated JJAS mean local Hadley circulation is compared with the observations for each model run. We notice that the RegCM-EE and RegCM-GE simulates stronger-than-observed (Fig. 3c, d) ascending motion over EIO (10°S–5°N) and north Indian Ocean (NIO) (5°N–15°N) regions which represents the regions of excessive amount of seasonal mean precipitation in the model over EIO and southern BoB region (Fig. 3c, d). Similarly, the deficit in precipitation is observed over CI region which is attributed to the absence of ascending motion after 15°N. In contrast, in RegCM-EG (Fig. 3b), the model simulated ascending motion is stronger than observed in 5–15°N latitudes over NIO which extends up to 20°N from the equator with rainfall maximum located over
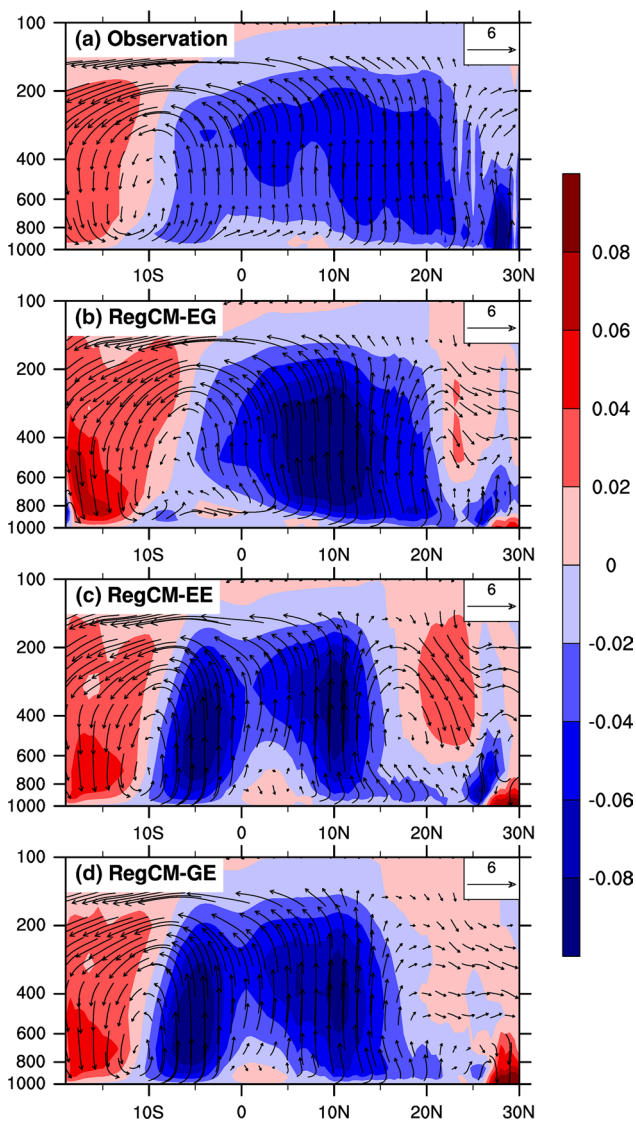
Fig. 3 Latitude-pressure sections of JJAS mean Hadley circulation averaged over (70–90°E). The *shading* denotes the magnitude of vertical velocity (Pa s^{-1}) multiplied with 100, **a** Observation, **b** RegCM-EG, **c** RegCM-EE, **d** RegCM-GE

eastern AS and southern BoB. Hence, the model simulated seasonal mean precipitation is observed more over NIO and is deficit near to the equator. The response of the monsoon precipitation in the model by different convective schemes is mainly due to modulation of the local Hadley cell which leads to unrealistic moisture transport. The unrealistic moisture transport in the model indicates the discrepancies in simulating the strength and proper location of maximum moisture transport zones such as AS and BoB as in observations which subsequently result in precipitation bias over the ISM region (Figure not shown).

To summarize the performance of the model to simulate the seasonal mean monsoon and its variability in

RegCM-EE, RegCM-EG and RegCM-GE, we have used Taylor diagram as shown in Fig. 4. The diagram provides a quick reference to how well the spatial/temporal variability matches each other in terms of their CC, root mean square error (RMSE), and the ratio of their variance (Taylor 2001). Since, we are testing the performance of the models against observations; the Taylor diagram depicts the statistics between the observed data and the model simulated parameters. The simulated variable with least RMSE, high CC and the normalized standard deviation (SD) close to unity (i.e. the model simulated variability is close to the observed variability), indicates the better performance of the model. In this analysis, we have considered the model simulated seasonal mean precipitation, 850 hPa zonal wind (U850) and surface specific humidity over ISM region (40°E–120°E, 15°S–30°N) and are assessed with reference to observations (Fig. 4). The distance from the origin indicates the normalized SD of each variable i.e. the ratio of SD of the variable in the model to the SD of the variable in the observations, while the cosine of the angle swept out by the position vector from the origin indicates the pattern correlation between observed and simulated variable. The distance from the reference point to a point on the diagram denotes the RMSE and is represented by concentric circles with reference point as its center. The circles of RMSE are drawn based on the skill score calculation using normalized SD and CC. The models exhibit distinctly different behavior in simulating U850, precipitation and specific humidity (Fig. 4). The simulation of U850 is reasonably well in each model with high CC ranging from 0.92 to 0.96, low RMSE and SD close to the observations. On the other
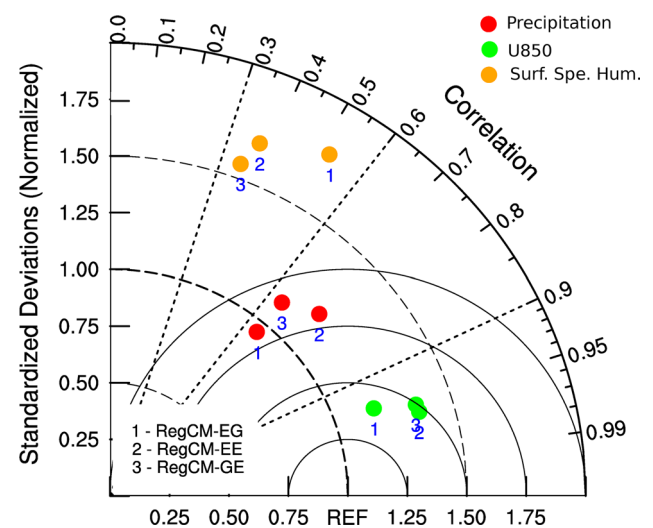
Fig. 4 Taylor diagram summarizing the model performances in simulating the mean meteorological fields such as low level wind, precipitation and surface specific humidity over ISM (40°–120°E and 15°S–30°N) region during boreal summer (JJAS)

Fig. 5 Probability distribution functions (PDF) for different rain rate categories, based on daily JJAS precipitation over, **a** central India (70°E–90°E; 18°N–28°N), **b** Bay of Bengal (86°E–94°E; 14°N–22°N), **c** Arabian Sea (68°E–74°E; 12°N–21°N), and **d** equatorial Indian Ocean (75°E–90°E; 10°S–0°)
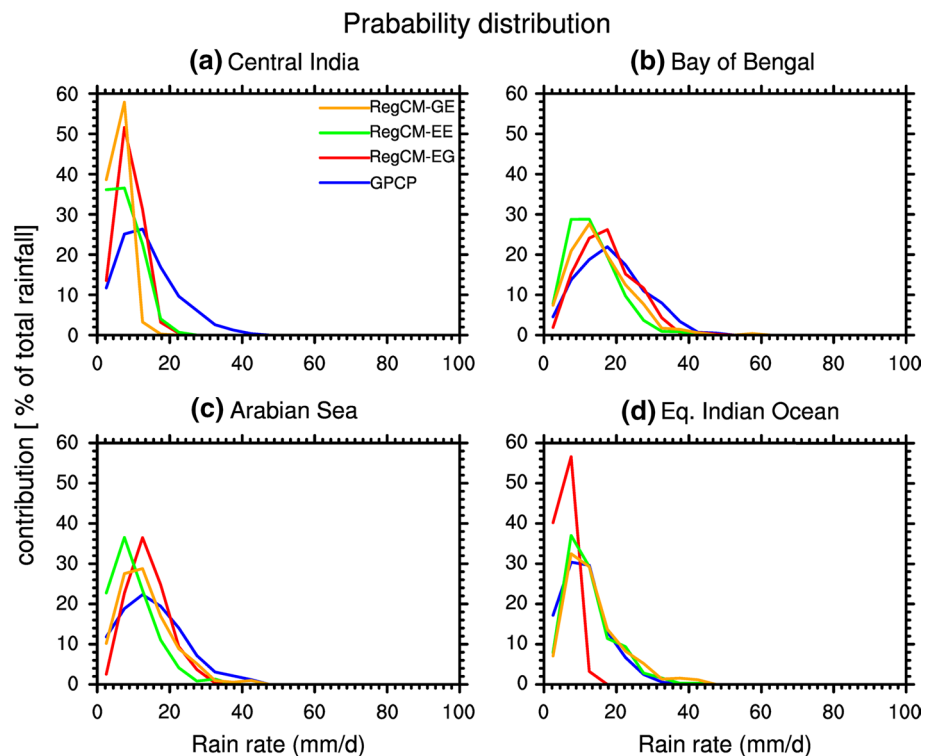
hand, precipitation bears moderate CC ranging from 0.62 to 0.76, moderate RMSE and SD are close to observations. However, the models are overestimating the surface specific humidity with low correlation (~0.3 to 0.5) and high RMSE. RegCM-EG simulated low level zonal winds and precipitation are better compared to RegCM-EE and RegCM-GE. It is evident that, RegCM-EG is more robust in simulating precipitation and winds in terms of correlation and variances (Fig. 4). All models fail to simulate proper distribution of surface specific humidity. Thus, considering both aspects (correlation and variance), RegCM-EG stands ahead among the other convective schemes in capturing the seasonal mean monsoon. Model experiments clearly indicate the representation of dynamics (circulation) is better than moist physics. Therefore, model needs further improvement in moist physics at sub grid-scale (e.g. cloud processes).

Further, we investigate how these biases reflect in simulation of various precipitation rates over convective regimes. Because, the accurate simulation of frequency distribution of rain rates is a precondition for the better simulation of mean state of monsoon as the precipitation follows the Poisson distribution (Abhik et al. 2013). Since the precipitation is discrete in nature, there exists large variability in their frequency, intensity and the amount of precipitation (Goswami et al. 2013). Therefore, a detailed analysis of precipitation characteristics is essential for realistic simulation of the mean state of the monsoon. To gain more insight among model performances, the observed

and simulated probability distribution functions (PDFs) of daily precipitation for monsoon season has been estimated over four convective heat source regions which are CI (70°E–90°E; 18°N–28°N), BoB (86°E–94°E; 14°N–22°N), AS (68°E–74°E;12°N–21°N) and EIO (75°E–90°E;10°S–0°). These regions are chosen based on climatology where major precipitation occurs. The PDF is computed for three different rain rate categories such as lighter (<10 mm day^{-1}), moderate (10–40 mm day^{-1}) and heavy (>40 mm day^{-1}) based on daily JJAS precipitation. The model simulated PDFs exhibits large difference compared with observed PDFs over these regions. Over CI region (Fig. 5a) the PDF of precipitation in all models show substantial overestimation of the lighter precipitation and underestimation of the moderate rain rate and no or negligible high precipitation rates compared to observations. The percentage contribution of lighter rain events to the total seasonal precipitation is nearly 20 % in observations whereas 40–60 % of precipitation is arising from lighter rain events in model experiments. This fact may be attributed partially to the underestimation of monsoon precipitation which arises due to the westward propagating lows or depressions from BoB region into CI region within the season. All models capture the PDFs of various precipitation categories as observed with more contribution arising from the moderate rain events over BoB (Fig. 5b) and over AS (Fig. 5c). A similar behavior is observed in RegCM-EG over the EIO region where the percentage contribution of lighter rain events is more with a complete absence

of moderate and heavy precipitation events whose effect is clearly seen in underestimating the seasonal mean precipitation over EIO region shown in Fig. 1. In contrast, the RegCM-EE and RegCM-GE simulates the PDFs reasonably well over EIO region with slight increase in percentage contribution in moderate and heavy rain events. From the above discussion, it is clear that the model has difficulty in simulating the PDF over CI region which represents the potential source of error where as it is relatively better over oceanic regions.

4 Simulation of monsoon intraseasonal oscillations

The primary goal of the study is to evaluate the sensitivity of RegCM for the simulation of MISOs for different convective parameterization schemes. In fact, the accurate representation of space–time characteristics of MISOs in the climate models is still remained a challenge. At first, to demonstrate how the magnitude and geographical distribution of intraseasonal variability over ISM region, the spatial distribution of total JJAS daily variance and 25–90 day filtered variance for both observation and model experiments have estimated in this study. Here, the amplitude of intraseasonal variability is the variance of 25–90 day

filtered daily precipitation anomalies during monsoon season. The spatial distribution of 25–90 day filtered variance and total JJAS daily variance from model and observations are shown in Fig. 6a–d. Observations (Fig. 6a) show high amplitude in intraseasonal variability primarily observed over ISM region namely; eastern AS, BoB, South China Sea, the western-north Pacific and the EIO. In comparison with observed intraseasonal variance over EIO, the model simulated intraseasonal variance is overestimated in RegCM-GE and RegCM-EE (Fig. 6c, d) and is underestimated in RegCM-EG (Fig. 6b). In contrast, the simulated intraseasonal variance over Indian subcontinent is low when compared with observations in each model. It is found that RegCM-EE is reasonably in good agreement with observed intraseasonal variance pattern, though it overestimates the amplitude over EIO. The Intraseasonal precipitation variance simulated from RegCM-EG (Fig. 6b) is close to observed variance over BoB and eastern CI but is absent over the EIO. On the other hand, RegCM-EE and RegCM-GE schemes (Fig. 6c, d) shows exaggerated unrealistic variance over EIO which resembles the seasonal precipitation bias in Fig. 1f, g. It is also noted that RegCM-GE could not produce ISO variance over CI region. Analysis suggests that the relationship between the mean and variance appears to be consistent with the fact that observed and simulated precipitation follows a Poisson
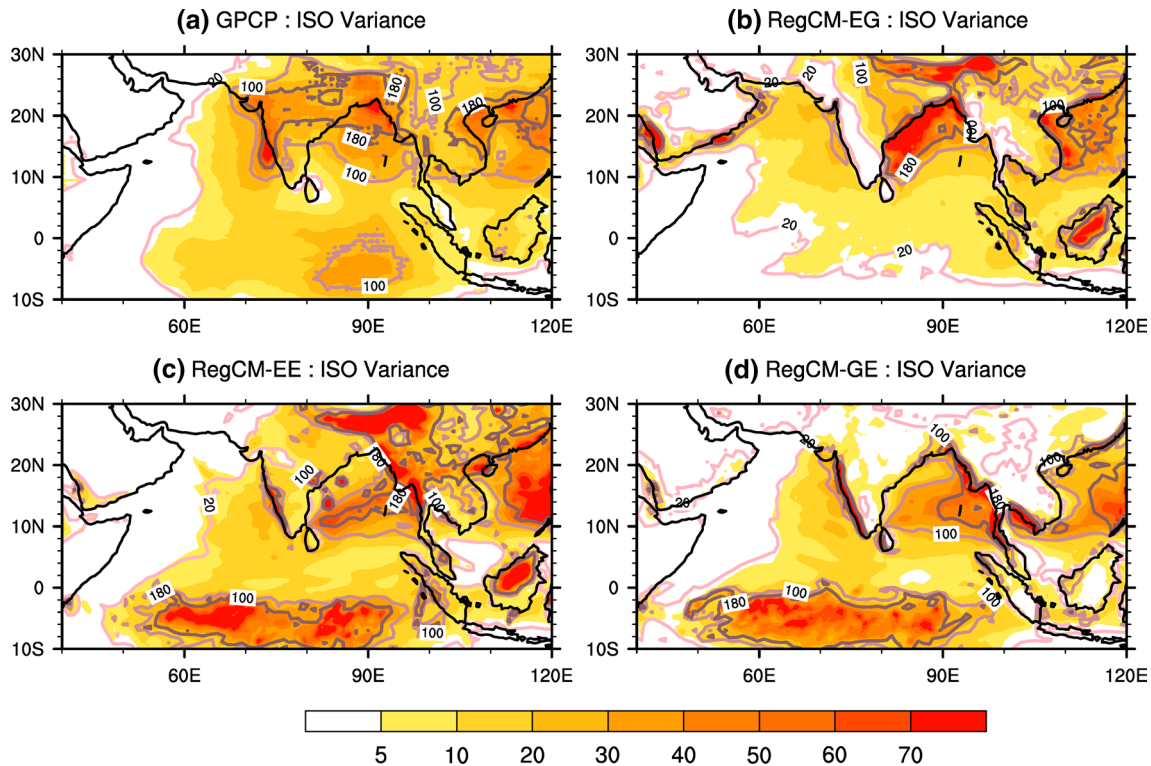

Fig. 6 The 25–90 day band pass filtered variance in precipitation ($mm^2\ day^{-2}$; *shaded*) and the total daily variance ($mm^2\ day^{-2}$; *contour*) during summer monsoon for **a** Observations, **b** RegCM-EG, **c** RegCM-EE, **d** RegCM-GE

distribution for which variance is proportional to the mean. It is observed that in three model experiments, the maximum zone of variance is misplaced and is co-located in the region of JJAS mean maximum precipitation zone which suggests the representation of mean monsoon rainfall is important for ISO variance. Overall the performance of RegCM-EE is superior to other two schemes on considering the entire monsoon domain.

During boreal summer, the dominant mode of MISOs is the slowly varying 30–50 day northward-propagating convection band. Therefore, the assessment of the model's ability to simulate these propagation characteristics of MISOs over ISM region is essential. Thus, we examine the model's fidelity in simulating the dominant mode of ISV during monsoon using wavenumber-frequency analysis (e.g. Hayashi 1982; Teng and Wang 2003; Fu et al. 2007; Goswami et al.

2013; Abhik et al. 2014). The analysis has been done over all latitudes so as to quantify the dominant mode of northward propagating variability over Indian sector. At first, the seasonal cycle has been removed from the data and it is averaged over the Indian longitudes 70°E–90°E. The spectra were calculated by performing complex Fast Fourier Transforms (FFTs) in time and latitude for each 184 day segment from May to October each year and then averaging over all the years. Figure 7 shows the wavenumber-frequency spectra of precipitation and low level zonal wind associated with monsoon intraseasonal variability averaged over Indian sub-continent for observation and the model experiments. In observations (Fig. 7a), meridional wavenumber 1 exhibits maximum spectral peak power at 40–50 day time scale in both precipitation and U850 wind. In addition to that, a strong coherence is observed between precipitation
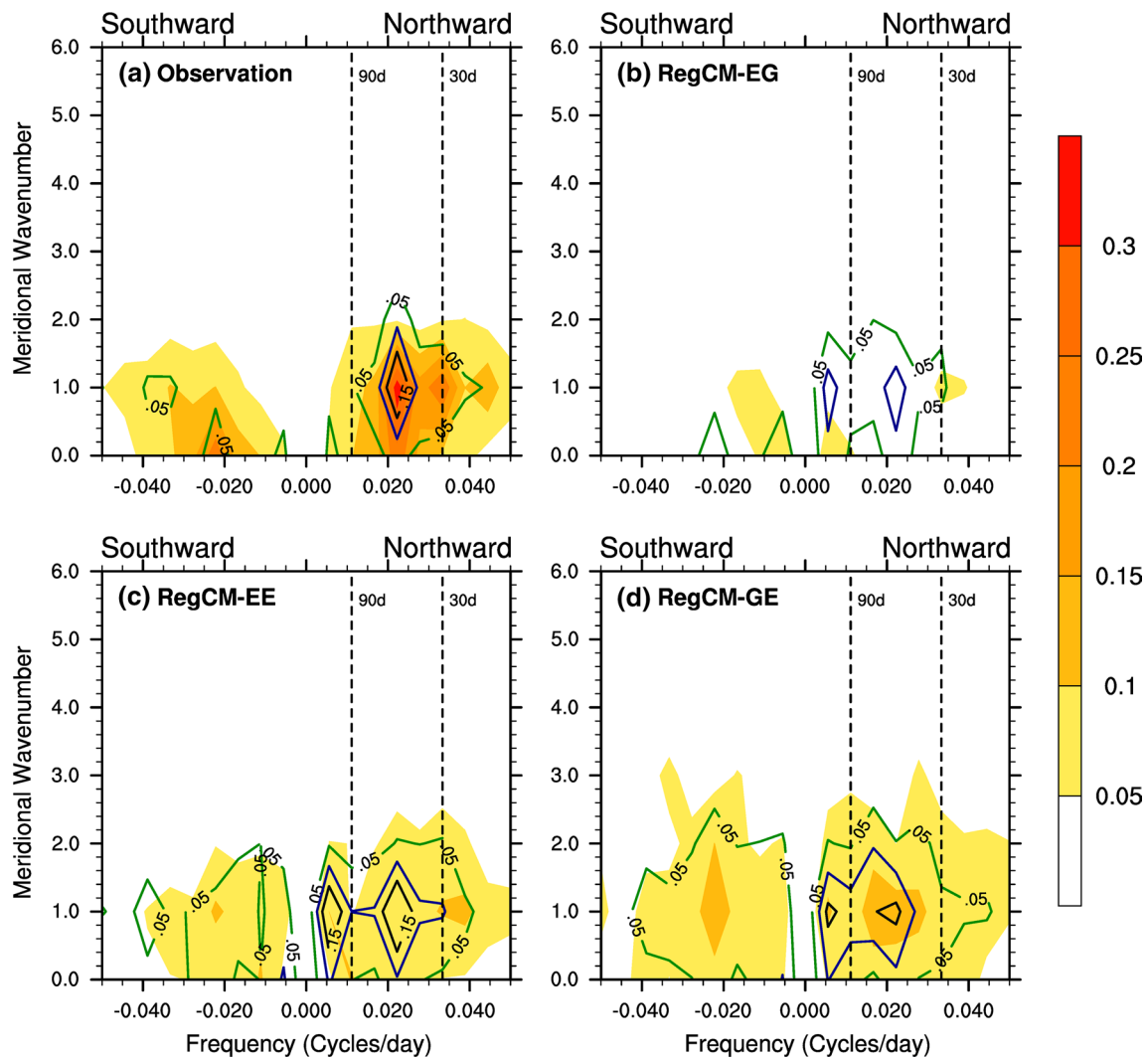
Fig. 7 Wavenumber—frequency spectra of precipitation (mm^2 day^{-2}, *colors*) and zonal wind (U850) (m^2 s^{-2}, *lines*) averaged over Indian longitudes (70–90°E) during boreal summer across the latitudes 15°S–30°N for **a** Observations, **b** RegCM-EG, **c** RegCM-EE, **d** RegCM-GE. The X-axis denotes frequency (cycles/day) and Y-axis denotes meridional wavenumber

and U850 wind variance. One can notice from Fig. 7 that, all model simulations show a preference for northward propagating disturbances in U850 wind with peak spectral power concentrated at meridional wavenumber 1, between 40–50 days similar to the observed spectra (Fig. 7a). However, the model produced spectral characteristics associated with precipitation are distinctly different from each other. The northward propagating intraseasonal mode in precipitation is completely absent in RegCM-EG where as RegCM-EE and RegCM-GE captured the observed spectra in precipitation with low spectral power. The model simulated spectral characteristics are very different in precipitation as well as zonal wind and exhibits lack of coherence between them in RegCM-EG where as relatively good coherence is observed in case of RegCM-EE and RegCM-GE (slightly higher wave number). It is important to mention that the coherence between wind and precipitation is very much needed in models to accurately reproduce the observed features of MISOs. On the whole, we can conclude that RegCM-EE and RegCM-GE are able to capture the northward propagating variability with low spectral power compared with observations. Out of these two models, RegCM-EE has shown relatively better performance compared with RegCM-GE (wider spectra) which captured the observed spatial and temporal scale of northward propagating variability and is consistent with Joseph et al. (2011) and Abhik et al. (2014).

4.1 Space–time evolution of MISOs

In this section, we further analyzed the space–time evolution characteristics of MISOs in both observation and the model experiments. Prior to the analysis of propagation

characteristics of MISOs, we analyzed the active and break composites of precipitation and low level wind anomalies since the active and break conditions are largely governed by dominant northward propagating MISO mode. These active and break spells are identified using ISO index and the identified active and break spells mostly match with previous studies (e.g. Rajeevan et al. 2010). However, the model identified active and break spells (Table 1) are mismatched (in terms of days) with observed spells, is consistent with Maharana and Dimri (2015). Realistic simulation of observed space–time characteristics of MISOs is important to test models ability to simulate the seasonal mean with fidelity. Figure 8 depicts the composites of active (left panel) and break (right panel) days of precipitation and low level winds for observation and model experiments. Observations (Fig. 8a) show strong southwesterly wind anomalies at lower level and excess precipitation over CI region during active condition. On the other hand, opposite is true for break composites with reduced convection over CI and increased convection over EIO (Fig. 8e). It is observed that the enhanced (suppressed) convection over CI (EIO) region is realistically represented in RegCM-EE (Fig. 8c, g) than other schemes during active (break) phases of ISM. We analyzed the spatial correlation of active and break composites fields of precipitation and wind against observations for all the models. During active phase, RegCM-EE bears high correlation of 0.6 and 0.7 respectively whereas it is 0.45 and 0.55 in the case of break composite. The other models show relatively less correlation in both active and break phases except for the break phase in RegCM-GE which shows little high correlation values i.e. 0.55 and 0.6. This analysis indicates that the performance of mixed

Table 1 The table lists the active and break spells identified by using ISO index derived from 25–90 day filtered precipitation anomalies

Year	GPCP		RegCM-EG		RegCM-EE		RegCM-GE	
	Active	Break	Active	Break	Active	Break	Active	Break
2001	2–12J	18–26J	7–22J	10–23A	28J–6A	15–31A	–	17–29A
2002	4–11A, 29–31A	3–15J	03–19J	30J–3A	9–18J	26–30J, 18–27A	–	1–18J
2003	19–29A	3–15A	12–22J, 26–31A	11–21A	5–12J	19J–2A	–	–
2004	29J–10A	17–23J, 27–31A	4–8J, 29J–8A	13–23J	6–11J, 5–13A	18–27J, 28–31A	9–20J	20–31A
2005	23–29J	7–12A, 24–31A	1–7J	15–22J, 5–11A, 29–31A	1–8J	3–11A	22–31J	9–15J, 7–17A
2006	1–6J	11–19J	26J–4A	10–19A	24J–6A	12–17J	20J–2A	
2007	1–6J, 1–7A, 27–31A	15–23J, 12–23A	1–4J, 16–31A	24J–7A	1–6J, 20–31A	12–19J	25–31A	11–18J, 10–16A
2008	–	9–18J, 18–31A	1–10J	–	24J–7A	11–19J	–	–
2009	1–19J, 29–31A	29J–9A	2–14J	3–12A	8–18J	25J–10A	1–15J, 25–31A	–
2010	22J–1A	10–17J, 7–17A	1–7J, 23–29J	11–18J, 5–9A	10–24J, 26–31A	30J–13A	–	5–21A
2011	12–21J, 29–31A	2–7J, 25J–3A, 17–21A	1–7J	–	5–14J, 21–31A	11–14A	1–7J, 11–17A	16–27J
2012	3–10J	3–8A	4–16J	7–14A	4–16J, 8–12A	20–30J	13–23J	–

The active (break) spells are identified if the ISO index is greater (less) than +1(−1) consecutively for a minimum period of 3 days. 'J' and 'A' indicate July and August months
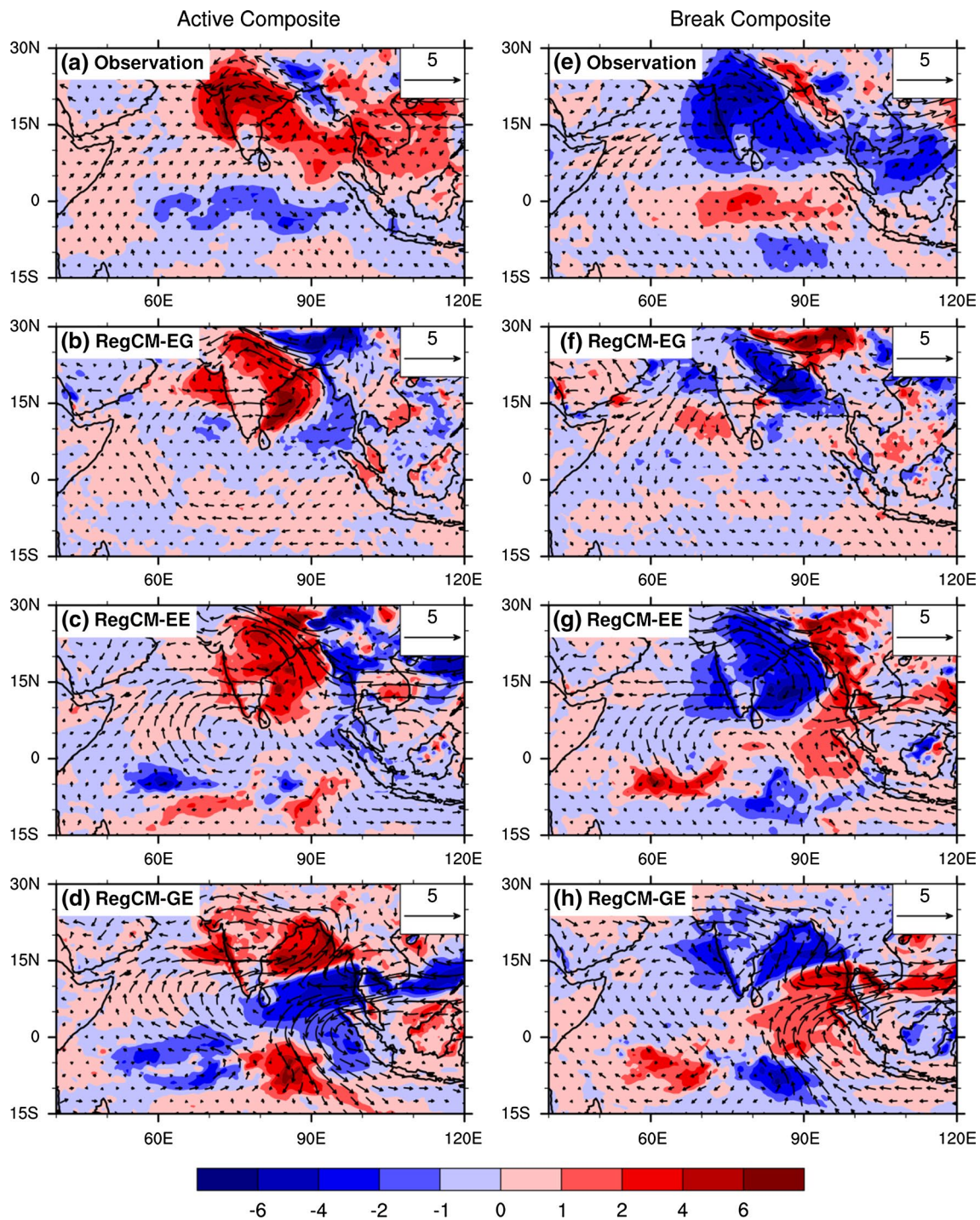
Fig. 8 Composites of precipitation (mm day^{-1}, *shaded*) and low level circulation (m s^{-1}, *vectors*, at 850 hPa) anomalies for active and break spells drawn for **a** observations, **b** RegCM-EG, **c** RegCM-EE and **d** RegCM-GE

convective schemes is distinctly different over ocean and land at intraseasonal time scales of ISM. Therefore, careful selection of convective schemes is indeed important for study the MISO in the model.

To examine the life cycle of the northward propagating MISOs, a lag-composite analysis has been performed on 25–90 day band pass filtered precipitation anomalies during JJAS. The identified MISO events are composited at different lags with reference to ISO index. Previous studies has noted that the half life cycle of the northward propagating MISOs can be resolved with a lag of 15 days (e.g. Suhas et al. 2012). Figure 9 depicts the space–time evolution of

the composite precipitation anomalies of MISOs from lag −15 to +15 days for observation and models. Day-0 represents the active monsoon condition with positive precipitation anomaly (enhanced convection) over CI region and day −15 or day +15 represents break monsoon condition with negative precipitation anomaly (suppressed convection). From Fig. 9a, it is clear that the convection first initiates over western Indian Ocean around day −15, and it extends eastward and then moves northwestward to Indian subcontinent in successive days. The initiation of convection in

the western EIO is preceded by surface wind convergence and central EIO warming (e.g. Wang et al. 2005). Around day-0, the convection sets over India, and it resembles the quadruple structure of MISO with eastward tilted rain band over Indian region extended up to the maritime continent, and suppressed convection over EIO and north Western Pacific (e.g. Annamalai and Slingo 2001). During the next half cycle, the positive precipitation anomalies over Indian subcontinent further move to the foothills of the Himalaya followed by negative precipitation anomalies from
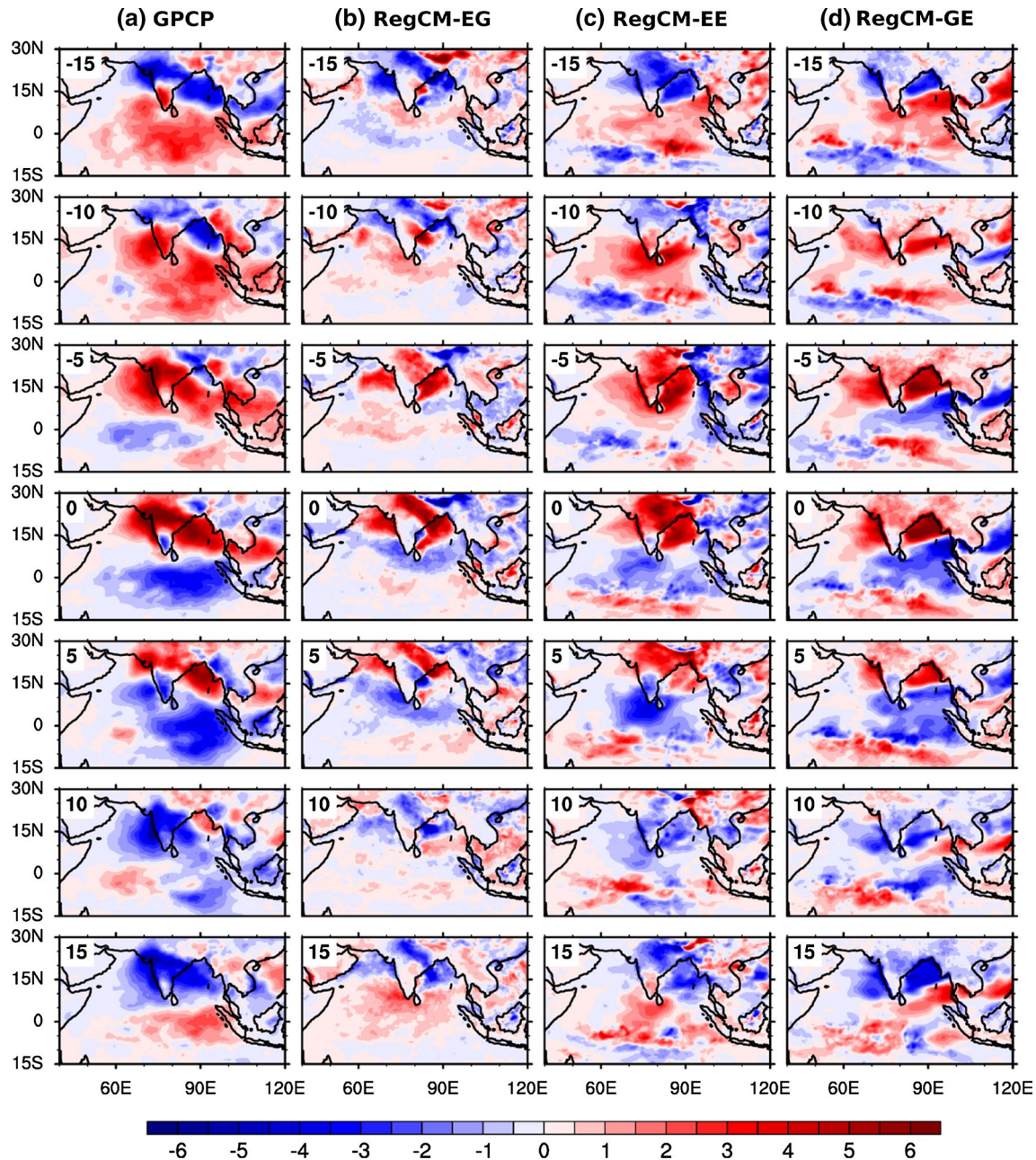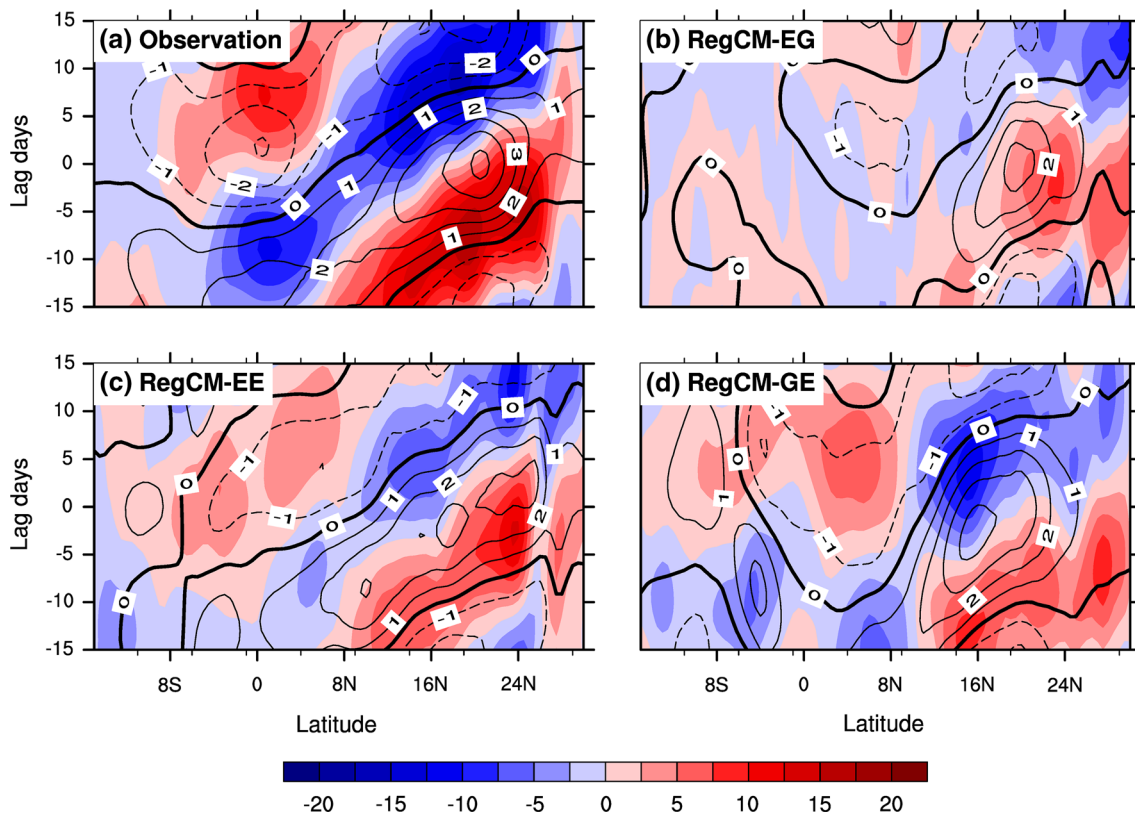

Fig. 9 Lag composite of 25–90 day band pass filtered precipitation anomalies (mm day^{-1}, *shaded*) with respect to ISO index for **a** GPCP, **b** RegCM-EG, **c** RegCM-EE, **d** RegCM-GE. Lag 0 represents the peak of the active spell identified using ISO index

EIO. It is evident from Fig. 9 that, the life cycle of MISO is reasonably well captured in RegCM-GE and RegCM-EE compared to observations where as in RegCM-EG, the EIO is completely void of variability at intraseasonal time scales. As we discussed in RegCM-GE, the precipitation anomalies are completely underestimated over the monsoon trough region during active/break condition, a similar underestimation is observed over Indian continent at all time lags during space–time evolution of MISOs. Therefore, RegCM-EE has the potential to simulate the space–time evolution characteristics of MISOs relatively better except that the model simulated precipitation anomalies are strongly confined to Indian region in contrast to observation where it extends up to northwest pacific region during both active and break phases of monsoon. The possible reason may be due to lack of eastward propagation of equatorial convection across the maritime continent during life-cycle of MISOs in all the model runs (Fig. 9b–d) and these discrepancies are still persists in many of global climate models (e.g. Zhu et al. 2010).

To get more insight into the possible reasons for the weak northward propagation of monsoon intraseasonal mode in models, we examine the vertically integrated

(surface to 100 hPa) horizontal moisture advection associated with MISOs during its life-cycle. The northward propagation of dominant MISOs is promoted by several mechanisms, but major contribution arises from boundary layer moisture advection. The magnitudes of northward propagating mechanisms vary from Indian Ocean to west Pacific Ocean (Demott et al. 2011). Figure 10, shows the lag composites (−15 days to +15 days) of 25–90 day filtered vertically integrated horizontal moisture advection and filtered precipitation anomalies averaged over Indian longitudes 70°E–90°E. Observations (ERAI & GPCP) clearly show the positive moisture advection from EIO into the CI region whose amount gradually increases from day −15 to day −0 (Fig. 10a). The positive moisture advection leads the positive precipitation anomalies from day −15 to day +15 during life-cycle of MISOs. It is known that, the positive moisture advection to the north of convection enhances the lower atmospheric instability which is one of the key features of the northward propagating MISOs (e.g. Jiang et al. 2004; Abhik et al. 2013). In RegCM-EG (Fig. 10b), the amount of moisture advection is completely underestimated during all phases of MISOs from day −15 to day +15. The moisture advection is better represented in

Fig. 10 Lag composite of 25–90 day band pass filtered precipitation anomalies (mm day^{-1}, *contour*) and vertical integrated horizontal moisture advection (Kg m^{-2} s^{-1}, *shaded*) with respect to ISO index and is averaged over Indian longitudes (70–90°E) for **a** observations, **b** RegCM-EG, **c** RegCM-EE, **d** RegCM-GE. The *black thick contour* indicates *zero line* and *solid line* for positive and *dashed line* for negative precipitation anomalies

RegCM-EE (Fig. 10c) and RegCM-GE (Fig. 10d) though the amount of moisture advection is relatively less compared with observations. This moisture advection process can be a possible reason for the dry bias observed over Indian sub-continent. The northward propagation of convection is little slower in RegCM-EE than the observed and the convection decays near 24°N. On careful examination, it is found that, RegCM-EE captured the true representation of moisture advection ahead of convection during all phases of its life-cycle which makes it suitable for the study of MISOs.

To study the propagation characteristics, lag regression analysis (as discussed in data and methodology) has been done with respect to ISO index. Figure 11 shows the hovmoller diagram of regressed precipitation anomalies at different lags averaged over Indian longitudes 70°–90°E for observation and model simulations. Observations (Fig. 11a) revealed clearly the origin and the propagation of precipitation anomalies in northward direction from EIO onto CI region with an average speed of 1.5° per day. Precipitation which was on equatorial region in lag-15 reaches central Indian region by lag 0 and extends further north. It is observed that, the models (Fig. 11b–d) exhibit a severe problem to generate high amplitude precipitation anomalies over EIO at intraseasonal time scale in comparable with observed (Fig. 11a) amplitude of precipitation anomalies.

Analysis of individual model performance confirmed that RegCM-EE (Fig. 11c) and RegCM-GE (Fig. 11d) captures relatively better northward propagation of precipitation anomalies over Indian latitudes though the precipitation anomalies are weaker over EIO. In RegCM-EE, the northward propagation of precipitation anomalies from EIO to CI region is in good agreement with observations whereas in RegCM-GE, the northward propagation takes longer period compared to observations. RegCM-EG (Fig. 11b) produces a standing oscillation of precipitation anomalies which might have arise due to locally generated convection over the Indian region. Thus the unrealistic propagation of MISO's in RegCM may indicate the lack of coherence between moist convective processes and internal atmospheric dynamics over ISM in the model. Therefore, on the whole we can infer that further improvement in representation of moist convective processes in RegCM-EE model can be able to capture the space–time evolution and propagation characteristics of MISOs during ISM.

4.2 Interannual variability of MISOs

In this section, we examined the performance of model in simulating the interannual variability (IAV) of MISOs for both observations and the model. The interannual variability of MISOs during the monsoon season is large and it
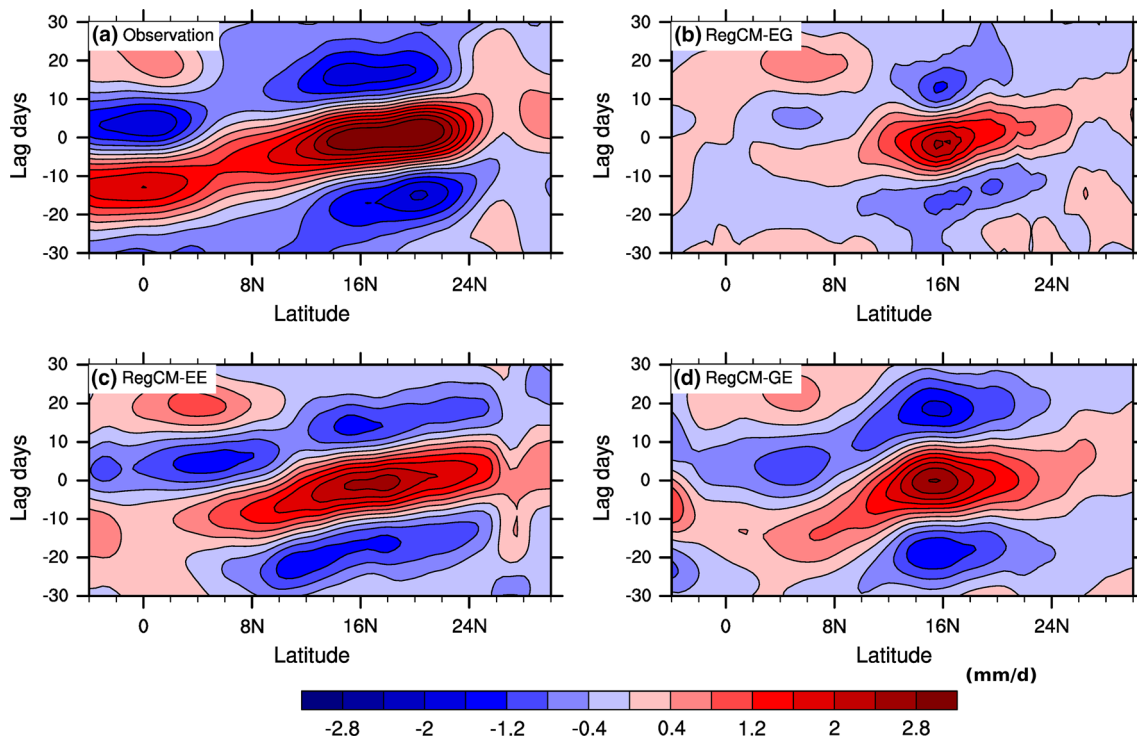

Fig. 11 Lag regression plot of 25–90 day band pass filtered precipitation anomalies (mm day^{-1}, *shaded*) regressed on ISO index for **a** GPCP, **b** RegCM-EG, **c** RegCM-EE and **d** RegCM-GE

responds differently to large scale phenomenon like Indian Ocean Dipole (IOD) and El Niño (e.g. Ajayamohan et al. 2009; Sharmila et al. 2014; Pillai and Chowdary 2015).

In order to examine the model performance of IAV of MISOs, we have chosen three El Niño developing years (2002, 2004 and 2009) and three El Niño decay years 2003, 2005 and 2007 during the study period and these years are selected based on Pillai and Chowdary (2015) study. In general, El Niño developing (decaying) years coincides with weak (strong/normal) monsoon years. Therefore, we

have considered 2003, 2005 and 2007 as strong/normal monsoon (SM) years and 2002, 2004 and 2009 as weak monsoon (WM) years. The intraseasonal variance is estimated for individual years using 25–90 day filtered rainfall and the spatial distribution of averaged variance for SM and WM years in displayed in Fig. 12. In Fig. 12a strong MISO variance over CI region, eastern AS, BoB, South China Sea, and the EIO during SM years is observed. On the other hand, the magnitude of MISO variance is weaker over CI region, EIO and eastern AS during WM years (Fig. 12e),
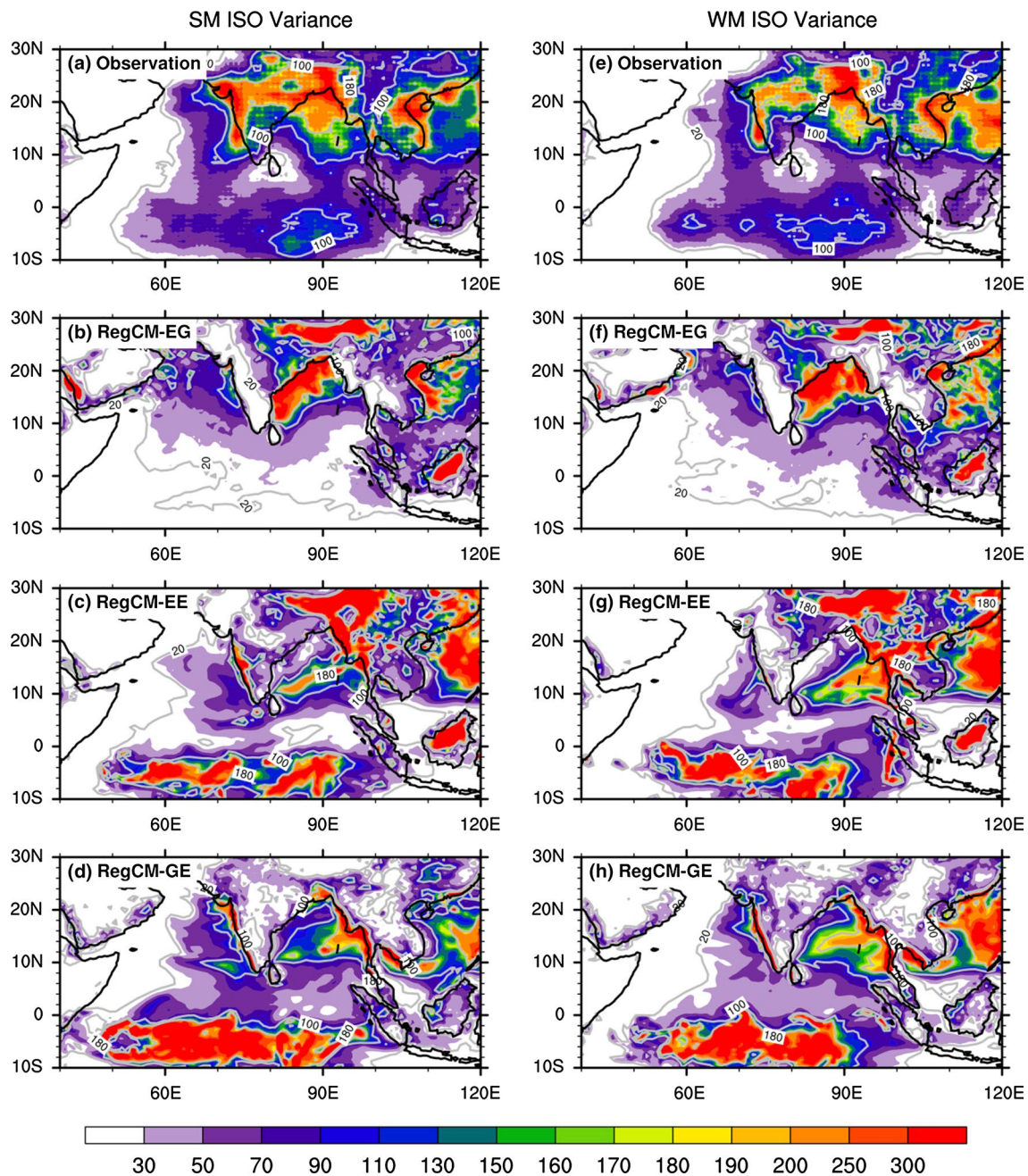

Fig. 12 The composite picture of spatial distribution of 25–90 day band pass filtered precipitation variance for strong monsoon (2003, 2005, 2007) and weak monsoon (2002, 2004, 2009) estimated for **a** observation, **b** RegCM-EG, **c** RegCM-EE and **d** RegCM-GE

which indicates that the intensity of MISO mode during extreme monsoons is different. RegCM-EG (Fig. 12b, f) show higher variance over BoB and no variance signal over EIO, eastern AS and CI region whereas RegCM-EE could simulate MISO variance (slightly underestimated) over eastern AS during SM (Fig. 12c) and WM (Fig. 12g).

RegCM-EE also could simulate the MISO variance over EIO but it extended towards west which resembles the seasonal mean rainfall. RegCM-GE completely missed the MISO variance over CI region though it produced better MISO variance over western pacific region during SM (Fig. 12d) and WM (Fig. 12f) compared to other schemes.
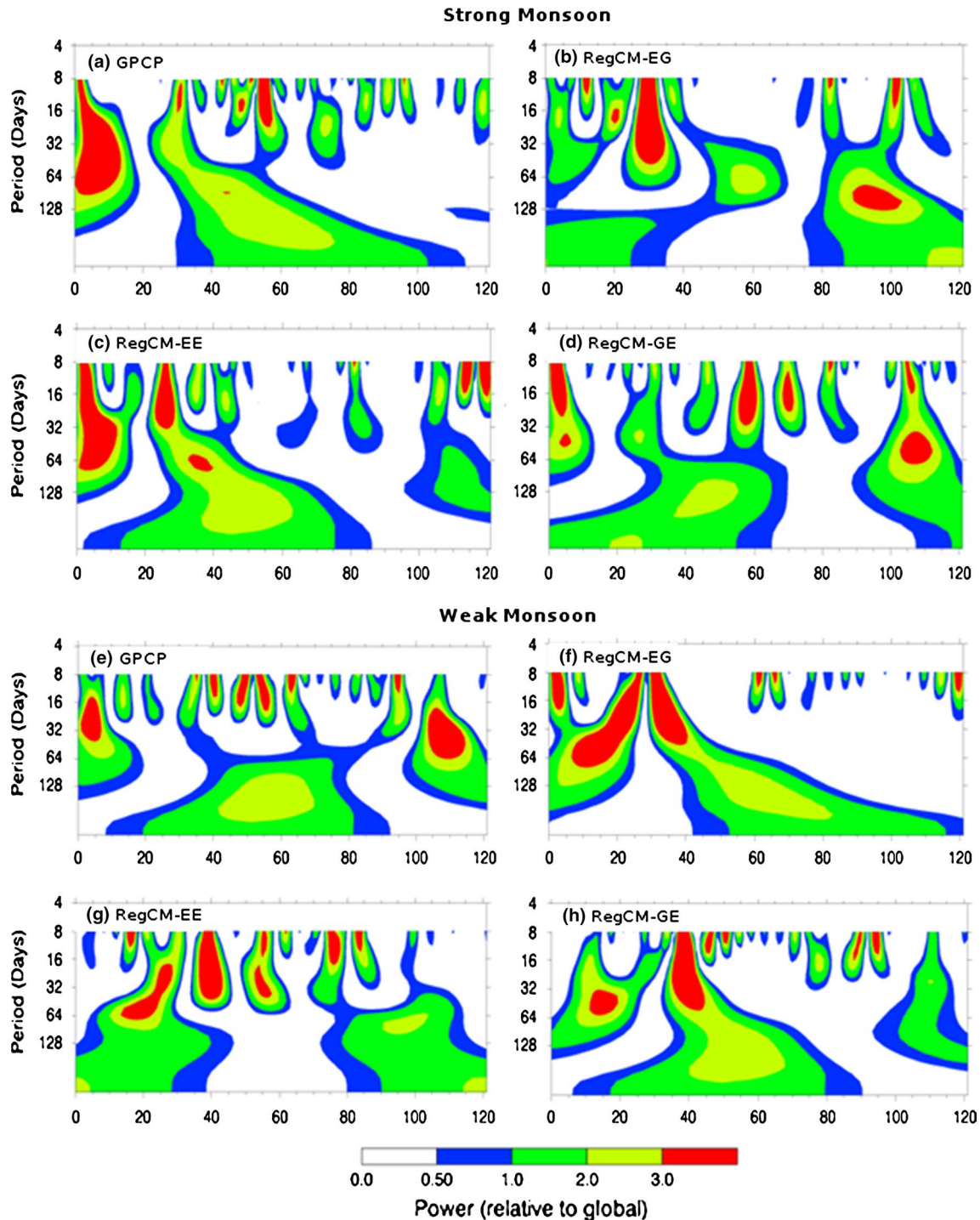
Fig. 13 Wavelet spectrum of JJAS precipitation over CI during strong and weak monsoon estimated for **a** GPCP, **b** RegCM-EG, **c** RegCM-EE and **d** RegCM-GE. The X-axis denotes days from 1 June to 30 September and Y-axis the period in power of two for wavelet spectrum

Further, we applied wavelet analysis on precipitation averaged over CI for analyzing localized variation of power within a time series. During SM, the spectrum shows the maximum variance centered at 25–90 days periodicity in the initial phase of monsoon (June) in the observations (Fig. 13a). With the progression of monsoon, the maximum

variance is located in the period <20 days, which is considered to be the dominant frequency during the SM years and these results are consistent with earlier studies (e.g. Kripalani et al. 2004; Singh and Oh 2007). RegCM-EE and RegCM-GE shows maximum variance in initial phase of monsoon (June) (Fig. 13c, d) like in observations whereas
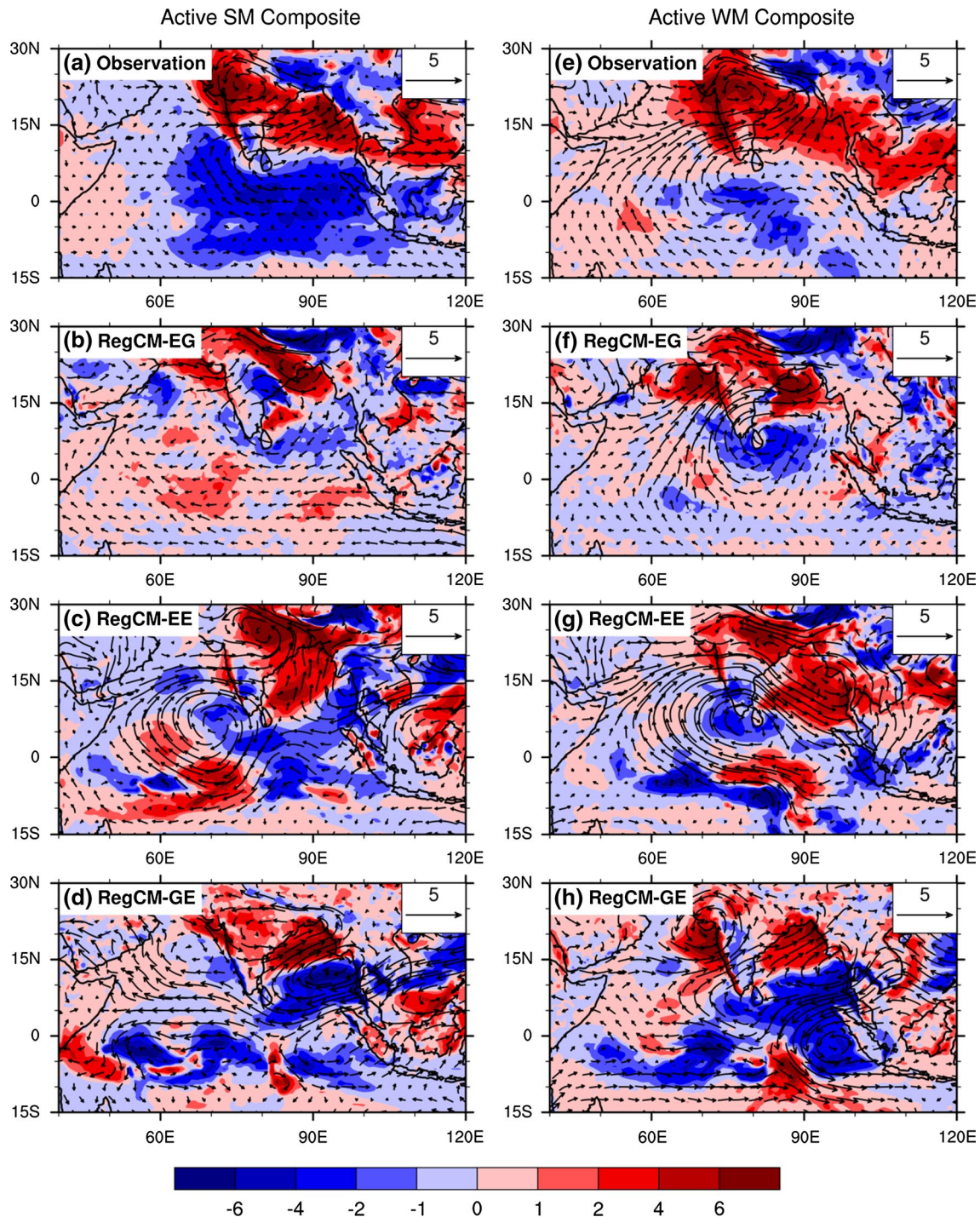
Fig. 14 The composites of precipitation anomalies (*shaded*; mm day^{-1}) and low level circulation anomalies (m s^{-1}, *vector*) at 850 hPa for active phase of **a** strong monsoon, **b** weak monsoon

RegCM-EG (Fig. 13b) shows the maximum variance in the first week of July (<40 days periodicity). It is also observed that RegCM-EG shows unrealistic maximum variance at the end of season unlike in observations. RegCM-EE (Fig. 13c) successfully simulates the high frequency oscillations in the first half of season, June-July; however, it is restricted below 60 days in the case of RegCM-GE which shows higher variance located at 60 days in withdrawal phase of monsoon. In the case of WM, the observed spectrum shows a center of maximum variance in the period between 10 and 30 days at the start (June) or withdrawal phase (September) of monsoon (Fig. 13e). Even in WM,
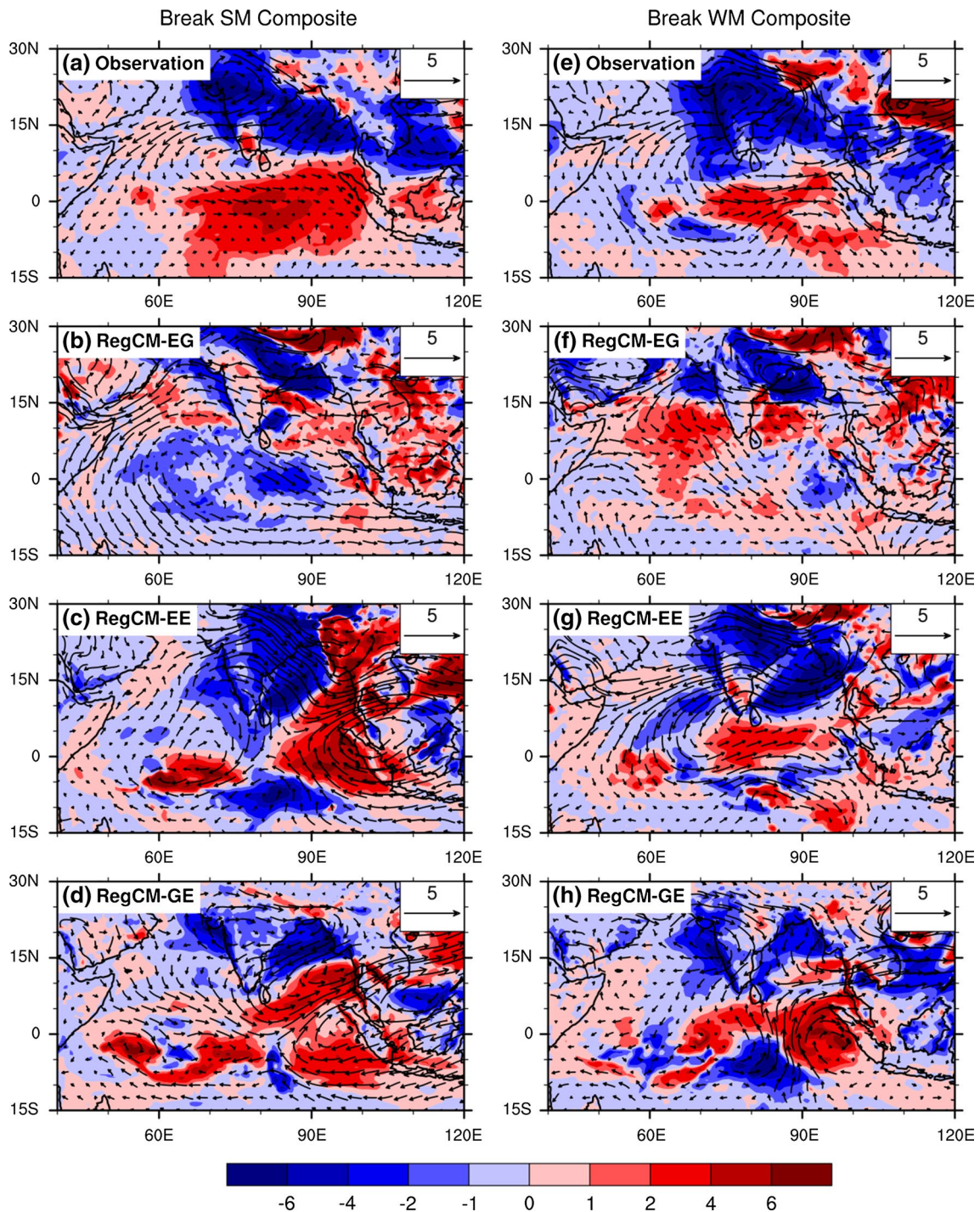
Fig. 15 The composites of precipitation anomalies (*shaded*; mm day^{-1}) and low level circulation anomalies (m s^{-1}, *vector*) at 850 hPa for break phase of **a** strong monsoon, **b** weak monsoon

the maximum variance is dominant in periods <20 days over central India during from July to August. These dominant periods show little higher spectral power compared with those in SM years. The models RegCM-EG (Fig. 13f) and RegCM-GE (Fig. 13h) failed to simulate the observed wavelet spectrum. On the other hand, RegCM-EE (Fig. 13g) shows relatively better distribution of MISO variances though it simulates dominant maximum variance at periods >20 days. Therefore, the RegCM-EE shows better interannual variability of MISOs than RegCM-GE and RegCM-EG.

Furthermore, the spatial structure of MISOs associated with the active and break spells of SM and WM years are examined using composite analysis. Figure 14 show composites of rainfall and low level circulation anomalies at 850 hPa for active phase of SM and WM. The active composite of SM (Fig. 14a) displays increased rainfall over ISM region and reduced rainfall over EIO. The increased rainfall over ISM region is linked to strong cyclonic circulation over Indian region. Compared to active composite of SM, WM composite (Fig. 14e) shows significant broad and well organized large scale convection over the Indian subcontinent associated with strong low level cyclonic circulation. It is also observed that, rainfall over BoB and EIO is relatively lesser than active composite of SM. It is important to mention that, the active composite of SM shows relatively weak low level cross equatorial flow compared to WM. According to Sharmila et al. (2014), the reason for that may be the difference in the frequency and duration of active phases of WM and SM, as the composites are averaged over the duration. RegCM-EG (Fig. 14b, f) could not able to produce enhanced (suppressed) convection over India (EIO) as in observations though it produces better circulation features in active composite of WM than SW. On the other hand, RegCM-EE (Fig. 14c, g) are slightly better in producing the rainfall and low level circulation over ISM region during active composite of SM and WM. However, it shows unrealistic anti-cyclonic circulation anomalies over southern tip of peninsular for both active composite of SM and WM. Finally, RegCM-GE (Fig. 14d, h) also shows similar nature like RegCM-EG in simulating the rainfall and circulation anomalies during active composite of SM and WM. Overall, it clearly indicates that the model has significant disparity in simulating convection and circulation during active composite of strong and weak monsoon. Compared to other convective schemes, RegCM-EE seems slightly better in simulating these features.

The composites of rainfall and low level circulation anomalies at 850 hPa for break phase of SM and WM shown in Fig. 15. Observations show that reduction in rainfall over Indian region, increased rainfall over east EIO during break composite of SM (Fig. 15a) and this reduction in rainfall over Indian region is associated with strong

anti-cyclonic circulation anomalies. On the other hand, the break composite of WM (Fig. 15e) looks similar to break composite of SM though the strength of precipitation anomalies over EIO is lesser than SM. These results support the findings of Pillai and Chowdary (2015). RegCM-EG (Fig. 15b, f) could not simulate the precipitation anomalies over EIO during break composite of SM and WM whereas it shows reduced rainfall anomalies over central Indian region and BoB. RegCM-EE (Fig. 15c, g) shows the realistic suppressed rainfall over Indian region in both SM and WM and also its associated anticyclonic circulation anomalies over the region simulated reasonably well compared to observations (Fig. 15e). It is also observed that RegCM-EE shows increased rainfall anomaly over EIO during break composite of WM like in observations whereas RegCM-EG, RegCM-GE (Fig. 15d, h) not able to simulate the proper geographical distribution of rainfall and circulation anomalies as in observations. Therefore, based on this analysis, we can conclude that among convective schemes, RegCM-EE is better in simulating the IAV of MISOs. However, it needs further improvement in simulating the IAV of MISOs in the model.

5 Summary and conclusions

In this study, the sensitivity of RegCM4.4 to the convective physics has been analyzed to simulate the seasonal mean and MISOs during ISM over south Asian CORDEX domain for RegCM-EG, RegCM-EE and RegCM-GE. The model simulated parameters are tested against GPCP and ERA interim reanalysis data throughout the analysis. The model performance has been tested to (1) simulate seasonal mean features, (2) simulate gross features of MISOs and (3) study the interannual variability of MISOs. Models have simulated several major circulation features of monsoon, though the magnitude of the simulated low level wind varies differently over land and ocean. A well organized cyclonic circulation over CI region (known as monsoon trough region) along the Indo-Gangetic plains is observed in RegCM-EG and is very weak in RegCM-EE and RegCM-GE. All three models produce more precipitation over the eastern AS, southern BoB and EIO regions expect RegCM-EG whose seasonal mean precipitation is close to observed value over EIO region. All models failed to simulate location of maximum rainfall band over the head BoB region and Myanmar coast, however, RegCM-EG simulated precipitation over CI and EIO region is relatively close to the observed mean value. The model (RegCM-EG) simulated seasonal cycle of precipitation over CI bears high correlation coefficient (0.81) against GPCP, whereas RegCM-EE and GE show low correlation values i.e. 0.49 and 0.68 respectively. A double ITCZ pattern is observed near the

equator with strong ascending motion on either side of it, and is observed in RegCM-EE, RegCM-GE which is most common in all types of climate models which is not observed in RegCM-EG. Over ISM, the model simulated seasonal mean values of zonal wind (850 hPa), precipitation, surface specific humidity bears high spatial correlation (0.92–0.96) for wind, moderate correlation (0.62–0.76) for precipitation and low correlation (~0.3 to 0.5) for surface specific humidity. As the range of correlation values is small, all models behave nearly similar; however, RegCM-EG keeps high correlation for all the variables over ISM. In RegCM-EG, PDFs of daily precipitation reveals that the major percentage of the seasonal mean rainfall over CI and EIO is arises from over estimation of low rain rate values unlike the observed PDFs in GPCP. All models behave closely over AS and BoB regions, where the model PDFs are closely following the observed PDFs with slight over estimation in the lighter and moderate rain events.

The intraseasonal variance of 25–90 day band pass filtered precipitation is co-located with the observed seasonal mean precipitation zone in all the models expect in RegCM-EG over EIO where the intraseasonal variance is very weak though the model simulated seasonal mean precipitation is close to the observed value. On the whole, the analysis suggests that, the representation of seasonal mean monsoon rainfall is important for accurate simulation of MISO variance. In observation, the meridional wavenumber 1 spatial scale exhibits maximum spectral peak power at 40–50 day time scale in both precipitation and U850 wind with a strong coherence observed between precipitation and U850 variance. The observed peak at 40–50 day scale in U850 is captured by all models with a slight change in amplitude of wind variance, however, the 40–50 day peak in precipitation is completely absent in RegCM-EG and RegCM-GE (lower magnitude)where as RegCM-EE captured it with low spectral power. The spatial correlation of active/break composite of precipitation and wind (U850) in model against observation shows that during active phase, RegCM-EE bears high correlation of 0.6 and 0.7 respectively whereas it is 0.45 and 0.55 in the case of break composite. The other models have shown relatively less correlation values compared to RegCM-EE. The lag composite analysis of observation clearly shows the origin of convection over western Equatorial Indian Ocean (WEIO) around day −15, and its evolution from WEIO which extends eastward and then moves northwestward to Indian subcontinent in successive days. The space–time characteristics of MISOs is reasonably well captured in RegCM-GE and RegCM-EE compared to observations whereas in RegCM-EG the intraseasonal variance is completely absent over oceanic regions throughout the life cycle.

The lag composite of 25–90 day filtered vertical integrated moisture advection shows positive moisture advection from EIO into the CI region whose amount gradually increases from day −15 to day −0. In RegCM-EG, the amount of moisture advection is completely underestimated during all phases of MISOs from day −15 to day −0 however, it is better represented in RegCM-EE and RegCM-GE with relatively less amount of moisture advection compared with observations. Since positive moisture advection to the north of convection enhances the lower atmospheric instability which is one of the key features of the northward propagating, we can conclude that, better representation of moisture advection leads to the improvement in the simulation characteristics of northward propagating MISOs. The lag regression analysis shows that, RegCM-EG produces a standing oscillation of precipitation anomalies which might have arise due to locally generated convection over the Indian region. In RegCM-EE, the northward propagation of precipitation anomalies from EIO to CI region is in good agreement with observations whereas in RegCM-GE, the northward propagation takes longer period compared to observations. Thus the unrealistic propagation of MISO's in RegCM may indicate the lack of coherence between moist convective processes and internal atmospheric dynamics over ISM in the model.

The characteristics of MISOs are studied for strong and weak monsoon years and the differences in model performances are analyzed. In observations the intraseasonal variance for SM and WM show various differences in their spatial distribution such as over CI, EIO and eastern AS large (small) amplitude of variance during SM (WM) monsoon years, over western pacific small (large) amplitude of variance during SM (WM) years, over BoB and South China Sea no change in variance. Though the models show large discrepancies in the simulation of mean intraseasonal variance compared to observation, the models respond slightly different in simulating intraseasonal variance under SM and WM years. The wavelet spectrum of rainfall averaged over CI depicts that, during SM the observations shows maximum variance centered around 25–90 days periodicity in the initial phase of monsoon (June) followed by periods <20 days which indicates that strong monsoon years are dominated with high frequency oscillations in a season. RegCM-EE and RegCM-GE shows maximum variance in initial phase of monsoon (June) like in observations, and RegCM-EE has simulated the high frequency oscillations like in observations. In the case of WM, the observed spectrum shows a center of maximum variance in the period between 10 and 30 days at the start (June) and little higher period at withdrawal phase (September) of monsoon. The maximum variance is dominant in periods <20 days during WM and these periods have more peak power compared to SM years. The models RegCM-EG and RegCM-GE fail to capture the high frequency periods whereas RegCM-EE captures relatively better.

The spatial structure of MISOs associated with the active and break spells of SM and WM years are examined by using composite analysis. In observations, compared to active composite of SM, WM composite shows (1) significant broad and well organized large scale convection over the Indian subcontinent associated with strong low level cyclonic circulation (2) strong low level cross equatorial flow (3) relatively less rainfall over BoB and EIO. In models, unrealistic precipitation distribution over CI and EIO in RegCM-EG, weak (void of) precipitation over CI in RegCM-EE (RegCM-GE) is observed. During break composite of SM and WM, in observations, reduced rainfall over CI, and increased rainfall over east EIO with a slight reduction in precipitation intensity over EIO in the case of WM is observed. RegCM-EE show realistic suppressed rainfall over CI in both SM and WM and its associated anticyclonic circulation whereas RegCM-EG, RegCM-GE not able to simulate the proper geographical distribution of rainfall and circulation as in observations. On the whole we can conclude that, the improvement in representation of moist convective processes over all intraseasonal time scales (3–7, 10–20 and 30–60 days) will simulate seasonal mean rainfall and also the space–time features of MISOs more realistically.

References

Abhik S, Halder M, Mukhopadhyay P, Jiang X, Goswami BN (2013) A possible new mechanism for northward propagation of boreal summer intraseasonal oscillations based on TRMM and MERRA reanalysis. Clim Dyn 40:1611–1624. doi:10.1007/s00382-012-1425-x

Abhik S, Mukhopadhyay P, Goswami B (2014) Evaluation of mean and intraseasonal variability of Indian summer monsoon simulation in ECHAM5: identification of possible source of bias. Clim Dyn 43:389–406

Ajayamohan RS, Rao SA, Luo JJ, Yamagata T (2009) Influence of Indian Ocean dipole on boreal summer intraseasonal oscillations in a coupled general circulation model. J Geophys Res 114:D06119. doi:10.1029/2008JD011096

Annamalai H, Slingo JM (2001) Active/break cycles: diagnosis of the intraseasonal variability of the Asian summer monsoon. Clim Dyn 18:85–102

Anthes RA, Kuo YH, Hsie EY, Low-Nam S, Bettge TW (1989) Estimation of skill and uncertainty in regional numerical models. Q J R Meteorol Soc 115:763–806

Bhaskaran B, Jones RG, Murphy JM, Noguer M (1996) Simulations of the Indian summer monsoon using a nested regional climate model: domain size experiments. Clim Dyn 12:573–587

Byun YH, Hong SY (2004) Impact of boundary layer processes on simulated tropical precipitation. J Clim 17:4032–4044

Dash SK, Shekhar MS, Singh GP (2006) Simulation of Indian summer monsoon circulation and precipitation using RegCM3. Theor Appl Climatol 86:161–172

Dee DP et al (2011) The ERA-Interim reanalysis: configuration and performance of the data assimilation system. Quart J R Meteorol Soc. 137:553–597. doi:10.1002/qj.828

Demott CA, Stan C, Randall DA, Klinter JL III, Khairoutdinov M (2011) The Asian monsoon in the superparameterized CCSM and its relationship to tropical wave activity. J Clim 24:5134–5156. doi:10.1175/2011JCLI4202.1

Duchon CE (1979) Lanczos filtering in one and two dimensions. J Appl Meteorol 18:1016–1022

Emanuel K (1991) A scheme for representing cumulus convection in large scale models. J Atmos Sci 48:2313–2335

Fu X, Wang B (2004) Different solutions of intraseasonal oscillation exist in atmosphere–ocean coupled model and atmosphere-only model. J Clim 17:1263–1271

Fu X, Wang B, Li T, McCreary JP (2003) Coupling between northward propagating intraseasonal oscillations and sea surface temperature in the Indian Ocean. J Atmos Sci 60:1733–1753

Fu X, Wang B, Waliser DE, Tao L (2007) Impact of atmosphere-ocean coupling on the predictability of monsoon intraseasonal oscillations. J Atmos Sci 64:157–174

Giorgi F (2006) Regional climate modeling: status and perspectives. J Phys IV 139:101–118. doi:10.1051/jp4:2006139008

Giorgi F, Marinucci MR, Bates GT (1993a) Development of a second generation regional climate model (REGCM2). Part I: boundary layer and radiative transfer processes. Mon Weather Rev 121:2794–2813

Giorgi F, Marinucci MR, Bates GT, DeCanio G (1993b) Development of a second generation regional climate model (REGCM2). Part II: convective processes and assimilation of lateral boundary conditions. Mon Weather Rev 121:2814–2832

Giorgi F et al (2012) RegCM4: model description and preliminary tests over multiple CORDEX domains. Clim Res 52:7–29

Goswami BN, Xavier PK (2003) Potential predictability and extended range prediction of Indian summer monsoon breaks. Geophys Res Lett 30(18):1966. doi:10.1029/2003GL017.810.2003

Goswami BN, Ajaya Mohan RS (2001) Intraseasonal oscillations and interannual variability of the Indian summer monsoon. J Clim 14:1180–1198

Goswami BN, Shukla J (1984) Quasi-periodic oscillations in a symmetric general circulation model. J Atmos Sci 41:20–37

Goswami BN, Wu G, Yasunari T (2006) The annual cycle, intraseasonal oscillations, and roadblock to seasonal predictability of the Asian summer monsoon. J Clim 19:5078–5098

Goswami BB, Mukhopadhyay P, Khairoutdinov M, Goswami BN (2013) Simulation of Indian summer monsoon intraseasonal oscillations in a superparameterized coupled climate model: need to improve the embedded cloud resolving model. Clim Dyn 41:1497–1507. doi:10.1007/s00382-012-1563-1

Grell GA (1993) Prognostic evaluation of assumptions used by cumulus parameterizations. Mon Weather Rev 121:764–787

Grenier H, Bretherton CS (2001) A moist PBL parameterization for large-scale models and its application to subtropical cloud-topped marine boundary layers. Mon Weather Rev 129:357–377

Hayashi Y (1982) Space-time spectral analysis and its applications to atmospheric waves. J Meteor Soc Jpn 60:156–171

Huffman GJ, Adler RF, Morrissey M, Bolvin DT, Curtis S, Joyce R, McGavock B, Susskind J (2001) Global precipitation at one degree daily resolution from multi-satellite observations. J Hydrometeorol 2:36–50

Jiang X, Li T, Wang B (2004) Structures and mechanisms of the northward propagating boreal summer intraseasonal oscillation. J Clim 17:1022–1039

Joseph S, Sahai AK, Chattopadhyay R, Goswami BN (2011) Can El Nino-Southern Oscillation (ENSO) events modulate intraseasonal oscillations of Indian summer monsoon? J Geophys Res 116:D20123. doi:10.1029/2010JD015510

Kiehl JT, Hack JJ, Bonan GB, Boville BA, Breigleb BP, Williamson D, Rasch P (1996) Description of the NCAR community climate model (CCM3). NCAR Tech. Note NCAR/TN-420+STR, 152 pp

Kripalani RH, Kulkarani A, Sabade SS, Revadekar JV, Patwardhan SK, Kulkarani JR (2004) Intraseasonal oscillation during monsoon 2002 and 2003. Curr Sci 87:325–331

Kripalani RH, Oh JH, Kulkarni A, Sabade SS, Chaudhari HS (2007) South Asian summer monsoon precipitation variability: coupled climate model simulations and projections under IPCC AR4. Theor Appl Climatol 90(3–4):133–159. doi:10.1007/s00704-006-0282-0

Krishna Kumar K, Hoerling M, Rajagopalan B (2005) Advancing dynamical prediction of Indian monsoon precipitation. Geophys Res Lett 32(8):L08704. doi:10.1029/2004GL021979

Krishnamurti TN, Subrahmanyam D (1982) The 30–50 day mode at 850 mb during MONEX. J Atmos Sci 39:2088–2095

Lawrence DM, Webster PJ (2002) The boreal summer intraseasonal oscillation: relationship between northward and eastward movement of convection. J Atmos Sci 59:1593–1606

Leung LR, Ghan SJ, Zhao ZC, Luo Y, Wang WC, Wei HL (1999) Intercomparison of regional climate simulations of the 1991 summer monsoon in eastern Asia. J Geophys Res 104:6425–6454

Lin R, Zhou T, Qian Y (2014) Evaluation of global monsoon precipitation changes based on five reanalysis datasets. J Clim 27(3):1271–1289

Maharana P, Dimri AP (2015) Study of intraseasonal variability of Indian summer monsoon using a regional climate model. Clim Dyn. doi:10.1007/s00382-015-2631-0

Oleson KW, NiuGy Yang ZL, Lawrence DM et al (2008) Improvements to the Community Land Model and their impact on the hydrologic cycle. J Geophys Res 113:G01021. doi:10.1029/2007JD000563

Pal JS, Small EE, Eltahir EAB (2000) Simulation of regional scale water and energy budgets: representation of sub-grid cloud and precipitation processes within RegCM4. J Geophys Res 105:29579–29594

Pal JS, Giorgi F, Bi X, Elguindi N, Solmon F, Gao X, Francisco R, Zakey A, Winter J, Ashfaq M, Syed F, Bell J, Diffenbaugh N, Karmacharya J, Konare A, Martinez-Castro D, Porfirio da Rocha R, Sloan L, Steiner A (2007) Regional climate modeling for the developing world: the ICTP RegCM3 and RegCNET. Bull Am Meteor Soc 88:1395–1409

Philippe LP et al (2011) Can regional climate models represent the Indian monsoon? J Hydrometeorol 12(5):849–868

Pillai PA, Chowdary JS (2015) Indian summer monsoon intra-seasonal oscillation associated with the developing and decaying phase of El Niño. Int J Climatol. doi:10.1002/joc.4464

Rajeevan M, Gadgil S, Bhate J (2010) Active and break spells of the Indian summer monsoon. J Earth Syst Sci 119(3):229–247

Rajeevan M, Rohini P, Niranjan Kumar K, Srinivasan J, Unnikrishnan CK (2013) A study of vertical cloud structure of the Indian summer monsoon using CloudSat data. Clim Dyn 40:637–650

Rajendran K, Kitoh A, Arakawa O (2004) Monsoon low-frequency intraseasonal oscillation and ocean-atmosphere coupling over the Indian Ocean. Geophys Res Lett. doi:10.1029/2003GL019031

Raju A, Parekh Anant, Chowdary JS, Gnanaseelan C (2015a) Assessment of the Indian summer monsoon in the WRF regional climate model. Clim Dyn 44:3077–3100. doi:10.1007/s00382-014-2295-1

Raju PVS, Bhatla R, Almazrouiand M, Assiri M (2015b) Performance of convection schemes on the simulation of summer monsoon features over the South Asia CORDEX domain using RegCM-4.3. Int J Climatol. doi:10.1002/joc.4317

Ratnam JV, Krishna Kumar K (2005) Sensitivity of the simulated monsoons of 1987 and 1988 to convective parameterization schemes in MM5. J Clim 18:2724–2743

Rupa Kumar K, Sahai AK, Krishna Kumar K, Patwardhan SK, Mishra PK, Revadekar JV, Kamala K, Pant GB (2006) High-resolution climate change scenarios for India. Curr Sci 90:334–345

Sharmila S, Joseph S, Chatopadhay R, Sahai AK, Goswami BN (2014) Asymmetry in space time characteristics of Indian summer monsoon intraseasonal oscillations during extreme years: role of seasonal mean state. Int J Climatol 35:1948–1963

Sikka DR, Gadgil S (1980) On the maximum cloud zone and the ITCZ over India longitude during the Southwest monsoon. Mon Weather Rev 108:1840–1853

Singh GP, Oh JH (2007) Impact of Indian Ocean sea surface temperature anomaly on Indian summer monsoon precipitation using a regional climate model. Int J Climatol 27:1455–1465. doi:10.1002/joc.1485

Slingo JM, Annamalai H (2000) 1997: the El Nino of the century and the response of the Indian Summer Monsoon. Mon Weather Rev 128:1778–1797

Suhas E, Neena JM, Goswami BN (2012) An Indian monsoon intraseasonal oscillations (MISO) index for real time monitoring and forecast verification. Clim Dyn 40:2605–2616. doi:10.1007/s00382-012-1462-5

Taylor KE (2001) Summarizing multiple aspects of model performance in a single diagram. J Geophys Res 106:7183–7192. doi:10.1029/2000JD900719

Teng H, Wang B (2003) Interannual variations of the boreal summer intraseasonal oscillation in the Asian-Pacific region. J Clim 16:3572–3584

Umakanth U, Kesarkar AP, Rao TN, Rao S (2014) An objective criterion for the identification of breaks in Indian summer monsoon precipitation. Atmos Sci Lett 16(3):193–198. doi:10.1002/asl2.536

Vernekar AD, Ji Y (1999) Simulation of the onset and intraseasonal variability of two contrasting summer monsoons. J Clim 12:1707–1725

Waliser DE et al (2003) AGCM simulations of intraseasonal variability associated with the Asian summer monsoon. Clim Dyn. doi:10.1007/s00382-003-0337-1

Wang B, Webster PJ, Teng H (2005) Antecedents and self-induction of the active-break Indian summer monsoon. Geophys Res Lett 32:L04704

Wang B, Webster P, Kikuchi K, Yasunari Qi Y (2006) Boreal summer quasi-monthly oscillation in the global tropics. Clim Dyn 27:661–675

Webster PJ, Magana VO, Palmer TN, Shukla J, Tomas RT, Yanai M, Yasunari T (1998) Monsoons: Processes, predictability and the prospects of prediction. J Geophys Res 103:14451–14510

Wu X, Liang X, Zhang GJ (2003) Seasonal migration of ITCZ precipitation across the equator: why Can't GCMs simulate it. Geophys Res Lett. doi:10.1029/2003GL017198

Yasunari T (1979) Cloudiness fluctuation associated with the northern hemisphere summer monsoon. J Meteor Soc Jpn 57:227–242

Yasunari T (1980) A Quasi stationary appearance of 30–40 day period in the cloudiness fluctuation during summer monsoon over India. J Meteor Soc Jpn 58:225–229

Zhang GJ, Mu M (2005) Simulation of the Madden-Julian oscillation in the NCAR CCM3 using a revised Zhang-McFarlane convection parameterization scheme. J Clim 18:4046–4064

Zhu W, Li T, Fu X, Luo JJ (2010) Influence of the Maritime Continent on the boreal summer intraseasonal oscillation. J Meteor Soc Jpn 88:395–407. doi:10.2151/jmsj.2010-308